Department of Energy
Albuquerque Operations Office
P.O. Box 5400
Albuquerque, New Mexico 87115

MAR 11 1988

FEDERAL EXPRESS 2426763894

Paul Lohaus
Acting Branch Chief
Low-Level Waste and Uranium
Recovery Project Branch, MS-623SS
U.S. NRC
1 White Flint North
11555 Rockville Pike
Rockville, MD 20552

Dear Mr. Lohaus:

The enclosed information is provided in response to a request made by Sandy Wastler in a telephone conversation with Richard Richey of my staff on March 10, 1988. We hope this information will be beneficial in your staff's review of the Green River Final Remedial Action Plan.

If you should have any questions, please contact Richard Richey at (505) 846-1210.

Sincerely,

W. John Arthur, III
Project Manager
Uranium Mill Tailings Project Office

Enclosure

cc w/o enclosure:
S. Wastler, NRC
D. Mann, DOE
B. Peel, TAC

Q_r = volume flux rate of alluvial groundwater beneath the tailings (resultant volume flux rate from mixing the background groundwater with the fluid percolating through the tailings) (gpm).

Q_t = volume flux rate (percolation) through the tailings (gpm).

C_t = concentration of water quality constituent in tailings pore fluid (lysimeter sample) (mg/l).

C_r = concentration of water quality constituent in the alluvium beneath the tailings (resultant concentration from mixing background alluvial water with tailings pore water) (mg/l).

Using Q_r = 9.9 gpm (see Table D.5.7), average pore water concentrations from lysimeter GRN01-714 (Table D.5.14), average background groundwater concentrations from alluvial monitor wells 563 and 707, and resultant groundwater concentrations from alluvial onsite wells 702, 704, and 705, Q_t was calculated to be 0.010 gpm using both uranium and manganese concentrations. Other constituents were considered but were not useful either because their background concentrations were higher than resultant concentrations or pore water analyses were not available.

Based on the calculated Q_t, the continuous infiltration rate over the eight-acre area of the tailings is 6.4 x 10^{-11} ft/s (2.0 x 10^{-9} cm/s); the average annual rate is equal to 0.024 in/yr (0.06 cm/yr), or 0.4 percent of the average annual precipitation. While this method of calculating Q_t has inherent uncertainties (e.g., averages are used and geochemical attenuation is not considered), it indicates that the percolation of water through the tailings is very little, and is probably within the range estimated by Rush et al. (1982). a) Detailed mixing calculations to estimate Q_t are on file in the UMTRA Project Office, Albuquerque, New Mexico.

Tailings pore water samples were collected and analyzed from lysimeter 714 located at the east end of the pile (see Figure D.5.1) in September, 1986, and March, 1987. Less than 500 milliliters could be obtained from the lysimeter each time, so only a select number of parameters could be analyzed. No pore water at all could be collected during an October, 1987, and January, 1988, sampling. Since radionuclide analyses require one liter or more, radionuclide concentrations in the pore water could not be determined. In addition, since only a select number of constituents were analyzed, a cation/anion balance could not be accurately performed and the reliability of the results are uncertain. Finally, the pore water samples are highly sensitive to fluctuations in soil moisture content (responses to rainfall and evaporation); this seems to be reflected by the high variance in pore water parameters like

JACOBS ENGINEERING

DATE 11-08-88 SUBJECT Tailings Source characterization SHEET NO. 1 of 7

BY LMC CHKD. JV JOB NO.

Tailings surface area - 8 acres (348,480 ft²)

→ Estimate the quantity of water moving through the existing tailings

Table B.2.23 Water-quality analysis for lysimeter 716, September, 1986, Green River, Utah, tailings site

Parameter	Parameter value	Detection limit
Ca	385	0.01
Cl	2900	1.0
K	16[ ]	0.01
Mg	1090	0.001
Na	111	0.002
NH_4	11	0.1
NO_3	2	1.0
SO_4	16000	0.1
TDS	26100	10.0
U	221	0.003

		714-01 03/12/87
PARAMETER	UNIT OF MEASURE	PARAMETER VALUE+/-UNCERTAINTY
ALUMINUM	MG/L	6300.
AMMONIUM	MG/L	14.
BORON	MG/L	0.5
CALCIUM	MG/L	457.
CHLORIDE	MG/L	113.
CHROMIUM	MG/L	2.61
FLUORIDE	MG/L	< 0.1
IRON	MG/L	2200.
MAGNESIUM	MG/L	2640.
MANGANESE	MG/L	360.
MOLYBDENUM	MG/L	0.2
NITRATE	MG/L	4500.
POTASSIUM	MG/L	0.19
SELENIUM	MG/L	0.092
SODIUM	MG/L	89.2
SULFATE	MG/L	56200.
TOTAL SOLIDS	MG/L	80800.
URANIUM	MG/L	675.

JACOBS ENGINEERING

DATE _____ SUBJECT on-site wells SHEET NO. 2 of 7

BY _____ CHKD. JL JOB NO. _____

Table B.2.22 Water-quality analyses for alluvial on-site wells 702, 704, and 705, Green River, Utah, tailings site

FORMATION OF COMPLETION: ALLUVIUM
HYDRAULIC FLOW RELATIONSHIP: ON SITE

PARAMETER	UNIT OF MEASURE	LOCATION ID - SAMPLE ID AND LOG DATE 702-01 06/07/86	702-01 09/07/86	702-02 09/07/86	702-03 09/07/86	702-04 09/07/86
		PARAMETER VALUE +/- UNCERTAINTY	PARAMETER VALUE +/- UNCERTAINTY	PARAMETER VALUE +/- UNCERTAINTY	PARAMETER VALUE +/- UNCERTAINTY	PARAMETER VALUE +/- UNCERTAINTY
ALKALINITY	MG/L CACO3	237.	245.	245.	245.	245.
ALUMINUM	MG/L	-	0.3	0.3	0.3	0.3
AMMONIUM	MG/L	24.	24.	24.	24.	24.
ANTIMONY	MG/L	-	< 0.003	< 0.003	< 0.003	< 0.003
ARSENIC	MG/L	< 0.01	< 0.01	< 0.01	< 0.01	< 0.01
BARIUM	MG/L	-	< 0.1	< 0.1	< 0.1	< 0.1
BORON	MG/L	-	0.4	0.4	0.4	0.4
CADMIUM	MG/L	-	< 0.001	< 0.001	< 0.001	< 0.001
CALCIUM	MG/L	499.	520.	520.	520.	520.
CHLORIDE	MG/L	93.	100.	100.	100.	100.
CHROMIUM	MG/L	-	0.02	0.02	0.02	0.02
COBALT	MG/L	-	< 0.05	< 0.05	< 0.05	< 0.05
CONDUCTANCE	UMHO/CM	3500.	3900.	3900.	3900.	3900.
COPPER	MG/L	-	0.03	0.03	0.03	0.03
FLUORIDE	MG/L	0.8	0.9	0.9	0.9	0.9
GROSS ALPHA	PCI/L	-	-	-	-	-
GROSS BETA	PCI/L	-	-	-	-	-
IRON	MG/L	0.07	< 0.03	< 0.03	< 0.03	< 0.03
LEAD	MG/L	-	< 0.01	< 0.01	< 0.01	< 0.01
MAGNESIUM	MG/L	122.	175.	175.	175.	175.
MANGANESE	MG/L	0.37	0.47	0.47	0.47	0.47
MERCURY	MG/L	-	< 0.0002	< 0.0002	< 0.0002	< 0.0002
MOLYBDENUM	MG/L	0.27	0.09	0.10	0.09	0.10
NICKEL	MG/L	-	0.05	0.05	0.05	0.05
NITRATE	MG/L	3.	440.	440.	440.	440.
NITRITE	MG/L	-	< 0.1	< 0.1	< 0.1	< 0.1
ORG. CARBON	MG/L	-	70.	70.	70.	70.
PB-210	PCI/L	-	4.4 1.6	3.5 1.6	4.0 1.4	4.2 1.9
PH	SU	7.34	6.81	6.81	6.81	6.81
PHOSPHATE	MG/L	-	< 0.1	< 0.1	< 0.1	< 0.1
PO-210	PCI/L	-	0.4 0.7	0.2 0.7	0.2 1.2	0.0 0.6
POTASSIUM	MG/L	11.7	14.8	14.8	14.8	14.8
RA-226	PCI/L	0. 0.1	0.1 0.2	0.1 0.2	0.1 0.2	0.1 0.2
RA-228	PCI/L	0. 0.9	0.0 1.0	0.8 1.0	0.0 1.0	0.0 0.8
SELENIUM	MG/L	< 0.005	0.100	0.099	0.099	0.100
SILICA	MG/L	-	9.	9.	9.	9.
SILVER	MG/L	-	< 0.01	< 0.01	< 0.01	< 0.01
SODIUM	MG/L	798.	800.	800.	800.	800.
STRONTIUM	MG/L	-	5.5	5.5	5.5	5.5
SULFATE	MG/L	3070.	2980.	2980.	2980.	2980.
TEMPERATURE	C - DEGREE	15.	20.	20.	20.0	20.
TH-230	PCI/L	-	1.1 1.1	1.8 0.8	1.6 0.8	1.9 0.9
TIN	MG/L	-	< 0.005	< 0.005	< 0.005	< 0.005
TOTAL SOLIDS	MG/L	5050.	5090.	5100.	5090.	5100.
URANIUM	MG/L	0.729	1.19	1.19	1.22	1.10
VANADIUM	MG/L	-	0.24	-	0.24	0.24
ZINC	MG/L	-	0.023	0.023	0.023	0.023

PARAMETER	UNIT OF MEASURE	LOCATION ID - SAMPLE ID AND LOG DATE 702-05 09/07/86	704-01 06/06/86	704-01 09/07/86	705-01 06/06/86	705-01 09/07/86
		PARAMETER VALUE +/- UNCERTAINTY	PARAMETER VALUE +/- UNCERTAINTY	PARAMETER VALUE +/- UNCERTAINTY	PARAMETER VALUE +/- UNCERTAINTY	PARAMETER VALUE +/- UNCERTAINTY
ALKALINITY	MG/L CACO3	247.	368.	390.	294.	298.
ALUMINUM	MG/L	0.3	-	0.3	-	0.4
AMMONIUM	MG/L	24.	41.	38.	27.	41.
ANTIMONY	MG/L	< 0.003	-	< 0.003	-	< 0.003
ARSENIC	MG/L	< 0.01	< 0.01	< 0.01	< 0.01	< 0.01
BARIUM	MG/L	< 0.1	-	< 0.1	-	< 0.1
BORON	MG/L	0.4	-	0.4	-	0.6
CADMIUM	MG/L	< 0.001	-	< 0.001	-	< 0.001
CALCIUM	MG/L	520.	463.	531.	456.	483.
CHLORIDE	MG/L	100.	258.	480.	321.	140.
CHROMIUM	MG/L	0.02	-	0.02	-	0.02
COBALT	MG/L	< 0.05	-	0.06	-	0.08
CONDUCTANCE	UMHO/CM	3900.	2850.	6100.	4900.	6200.
COPPER	MG/L	0.03	-	0.04	-	0.04
FLUORIDE	MG/L	0.9	1.1	1.2	0.8	0.8
GROSS ALPHA	PCI/L	-	200. 110.	-	-	-
GROSS BETA	PCI/L	-	180. 60.	-	-	-
IRON	MG/L	< 0.03	0.09	0.03	0.07	0.06
LEAD	MG/L	< 0.01	-	< 0.01	-	< 0.01
MAGNESIUM	MG/L	175.	231.	247.	268.	316.
MANGANESE	MG/L	0.47	0.90	0.48	0.02	0.03
MERCURY	MG/L	< 0.0002	-	< 0.0002	-	< 0.0002
MOLYBDENUM	MG/L	0.10	0.25	0.14	0.24	0.16
NICKEL	MG/L	0.05	-	0.05	-	0.10
NITRATE	MG/L	440.	20.	250.	5.	22.
NITRITE	MG/L	< 0.1	-	< 0.1	-	< 0.1
ORG. CARBON	MG/L	70.	104.	70.	-	-
PB-210	PCI/L	5.2 1.7	1. 0.9	1.5 1.7	7.46	7.31
PH	SU	6.81	7.16	7.11	-	< 0.1
PHOSPHATE	MG/L	< 0.1	-	< 0.1	-	-
PO-210	PCI/L	0.3 0.7	0.4 0.6	0.0 0.6	19.4	20.4
POTASSIUM	MG/L	14.8	18.7	29.0	-	-
RA-226	PCI/L	0.2 0.2	-	0.0 0.2	-	-
RA-228	PCI/L	0.0 0.8	-	0.0 1.1	-	18.
SELENIUM	MG/L	0.100	< 0.005	0.092	< 0.005	< 0.005
SILICA	MG/L	9.	-	10.	-	7.
SILVER	MG/L	< 0.01	-	< 0.01	-	< 0.01
SODIUM	MG/L	800.	1290.	2010.	2100.	2090.
STRONTIUM	MG/L	5.5	-	6.6	-	6.6
SULFATE	MG/L	2980.	4200.	5290.	6930.	6420.
TEMPERATURE	C - DEGREE	20.	15.	22.	15.	18.
TH-230	PCI/L	2.8 1.0	0. 0.2	1.1 0.7	-	< 0.005
TIN	MG/L	< 0.005	-	< 0.005	-	9730.
TOTAL SOLIDS	MG/L	5090.	8480.	8490.	9780.	0.0485
URANIUM	MG/L	1.16	0.407	0.280	0.0419	0.21
VANADIUM	MG/L	0.24	-	0.24	-	0.027
ZINC	MG/L	0.021		0.025		

FORM 91-005 1 (4/81)

Table B.2.21 Concentrations of major and trace constituents in groundwater, Green River, Utah, tailings site

FORMATION OF COMPLETION: ALLUVIUM
HYDRAULIC FLOW RELATIONSHIPS: UP GRADIENT

PARAMETER	UNIT OF MEASURE	LOCATION ID - SAMPLE ID AND LIKE DATE: 561-01 08/04/86 — PARAMETER VALUE +/- UNCERTAINTY	561-01 09/07/86 — PARAMETER VALUE +/- UNCERTAINTY	707 01 08/04/86 — PARAMETER VALUE +/- UNCERTAINTY	707-01 09/07/86 — PARAMETER VALUE +/- UNCERTAINTY		PARAMETER VALUE +/- UNCERTAINTY
ACIDALKITY	MG/L CACO3	157.	182.	360.	176.		
ALUMINUM	MG/L	0.4	0.3	0.4	0.2		
AMMONIUM	MG/L	< 0.1	< 0.1	< 0.1	2.4		
ANTIMONY	MG/L	< 0.003	< 0.003	< 0.003	< 0.003		
ARSENIC	MG/L	< 0.01	< 0.01	< 0.01	< 0.01		
BALANCE	I	0.16	0.06	-1.20	0.18		
BARIUM	MG/L	0.2	0.2	0.3	< 0.1		
BORON	MG/L	0.3	0.5	0.6	0.4		
CADMIUM	MG/L	< 0.001	< 0.001	< 0.001	< 0.001		
CALCIUM	MG/L	486.	500.	488.	520.		
CHLORIDE	MG/L	312.	240.	312.	690.		
CHROMIUM	MG/L	0.05	0.02	0.05	0.02		
COBALT	MG/L	0.09	0.07	0.09	0.07		
CONDUCTANCE	UMHO/CM	5500.	6250.	4900.	6290.		
COPPER	MG/L	0.05	0.03	0.05	0.04		
FLUORIDE	MG/L	0.6	0.7	0.6	0.7		
IRON	MG/L	0.18	0.20	0.18	0.04		
LEAD	MG/L	< 0.01	< 0.01	< 0.01	< 0.01		
MAGNESIUM	MG/L	364.	367.	368.	388.		
MANGANESE	MG/L	0.04	0.03	0.04	0.03		
MERCURY	MG/L	< 0.0002	< 0.0002	< 0.0002	< 0.0002		
MOLYBDENUM	MG/L	0.15	0.14	0.18	0.06		
NICKEL	MG/L	0.04	< 0.04	0.09	0.08		
NITRATE	MG/L	11.	11.	11.	120.		
NITRITE	MG/L	< 0.1	< 0.1	< 0.1	< 0.1		
ORG. CARBON	MG/L	-	-	-	41.		
PB-210	PCI/L	-	-	-	0.0	1.3	
PH	SU	7.69	7.55	7.88	7.56		
PHOSPHATE	MG/L	< 0.1	< 0.1	< 0.1	< 0.1		
PO-210	PCI/L	-	-	-	0.0	0.6	
POTASSIUM	MG/L	18.8	22.6	19.3	26.1		
RA-226	PCI/L	-	-	0.2 0.2	0.2	0.2	
RA-228	PCI/L	-	-	1.1 0.9	0.0	0.8	
SELENIUM	MG/L	< 0.005	< 0.005	< 0.005	0.049		
SILICA	MG/L	4.	7.	4.	8.		
SILVER	MG/L	< 0.01	< 0.01	< 0.01	< 0.01		
SODIUM	MG/L	1680.	1830.	1680.	2090.		
STRONTIUM	MG/L	7.2	8.6	7.2	6.3		
SULFATE	MG/L	5540.	5960.	5530.	6070.		
TEMPERATURE	C - DEGREE	19.	17.	15.	19.		
TH-230	PCI/L	-	-	-	0.8	1.6	
TIN	MG/L	< 0.005	< 0.005	< 0.005	< 0.005		
TOTAL SOLIDS	MG/L	9230.	8800.	9420.	9480.		
URANIUM	MG/L	0.0121	0.0104	0.0175	0.0090		
VANADIUM	MG/L	0.17	0.22	0.29	0.14		
ZINC	MG/L	0.026	0.131	0.073	0.023		

B-92

URANIUM

C_b = Background = 0.0118 mg/l (wells 563 ; 707)

C_a = On Site = 0.466 mg/l (wells 702, 704, ; 705)

C_t = Pore Water = 448 mg/l (lysimeter 716 ave of 9-86 ; 3-87)

$q_b = q_a - q_t$

$\bar{q}_t = \frac{9.9}{37.8}$ gpm

find q_t

a = alluvium (laundry pile)
b = background
t = tailings

$$C_b(q_a - q_t) + C_t q_t = C_a(q_a)$$

$$C_b q_a - C_b q_t + C_t q_t = C_a q_a$$

$$C_a q_a - C_b q_a = -C_b q_t + C_t q_t$$

$$C_a q_a - C_b q_a = C_t q_t - C_b q_t$$

$$0.466\left(\frac{9.9}{37.8}\right) - 0.0118\left(\frac{9.9}{37.8}\right) = 448\, q_t - 0.0118\, q_t$$

$$\frac{4.613}{15.28} - \frac{0.117}{0.39} = 447.99\, q_t$$

$$4.613 - 0.117 = 447.99\, q_t$$

$$q_t = \frac{0.010}{0.033}\ \text{gpm}$$

NITRATE

C_b = 55 mg/l (wells 563; 707)

C_a = 140 mg/l (wells 702, 704, ; 705)

C_t = (2+4500) ÷ 2 = 2251 mg/l — too variable

Q_a = 32.8 gpm

$C_a Q_a - C_b Q_a = C_t Q_t - C_b Q_t$

$140(32.8) - 55(32.8) = 2251 Q_t - 55 Q_t$

$4592 - 1804 = 2196 Q_t$

$2788 = 2196 Q_t$

$Q_t = 1.27$ gpm

Sulfate

C_b = 5775 mg/l (wells 563 + 707)

C_a = 4648 mg/l (wells 702, 704, 705)

won't work

TDS

won't work

Manganese

C_b = 0.035 mg/l (wells 563 ; 707)

C_a = 0.39 mg/l (wells 702, 204, 705)

q_a = ~~320~~ 9.9 gpm C_t = 360 mg/l (lysimeter 3-07)

$$(C_a - C_b) q_a = (C_t - C_b) q_t$$

$$q_t = \frac{(C_a - C_b) q_a}{(C_t - C_b)}$$

$$q_t = \frac{(0.39 - 0.035)\ 9.9}{360 - 0.035}$$

$$q_t = \frac{3.51}{359.97} = 0.010 \text{ gpm}$$

~~$q_t = \frac{11.54}{359.97} = 0.032$ gpm~~

for q_t = 0.010 ~~0.032~~ gpm.

area of pile = 348,480 ft^2 = 8 ac

0.010 ~~0.032~~ gpm = 2.2×10^{-5} ~~7.2×10^{-5}~~ cfs ✓ (1.2×10^{-5})

($.033$ gpm = 2.13×10^{-5} cfs : 6.49×10^{-11} ft/sec)

2.2×10^{-5} ~~7.2×10^{-5}~~ cfs ÷ 348,480 ft^2 = 6.39×10^{-11} ~~2.07×10^{-10}~~

= ~~6.30×10^{-9}~~ cm/sec

= 1.95×10^{-9}

1.95×10^{-9} cm/sec = 0.06 cm/yr

~~6.30×10^{-9} cm/sec = 0.20 cm/yr~~ 6 in/yr = 15.24 cm/yr : arc annual precip

JACOBS ENGINEERING

DATE _____ SUBJECT _____ SHEET NO. 7 of 7

BY YMC CHKD. JC JOB NO. _____

$$\text{ratio} = \frac{0.06}{0.20} \text{ cm/yr} \Big/ 15.24 \text{ cm/yr}$$

$0.013 = 1.3\%$

$0.004 = 0.4\%$

Saturated K of tailings = 5.8×10^{-4} cm/sec
$= 1.9 \times 10^{-5}$ ft/sec

no way $\Longrightarrow$ $q = 1.9 \times 10^{-5}$ ft/s $(398,710 \text{ ft}^2) = 6.63$ cfs
$= 2976$ gpm

Assume $q_L = \frac{0.040 \text{ gpm}}{0.032 \text{ gpm}}$

annual precipitation evaporates back into the atmosphere and long-term drainage off the pile would be negligible. Finally, since the long-term seepage rate through the tailings is estimated to be 1 x 10^{-8} cm/s (or 1 x 10^{-7} cm/s at the most), ponding or "bathtubbing" of seepage in the disposal cell will not occur. (b) Detailed runoff and ponding calculations are on file at the UMTRA Project Office, Albuquerque, New Mexico.

D.5.4.2 Seepage Impacts

Mixing and dilution

Following percolation downward through the fractured foundation bedrock, tailings seepage will contact and mix with groundwater flowing beneath the disposal cell. The upper-middle shale unit is probably not saturated beneath the southern sector of the disposal cell (See Figure D.5.4). Fo this reason it is assumed that tailings seepage will mix with groundwater in both the upper-middle and lower-middle units beneath the cell, and in approximately equal proportions. The mixing is assumed to take place in the saturated thickness of the upper-middle unit beneath the cell (maximum of ten feet), and in the saturated thickness of the lower-middle unit beneath the cell (20 feet).

Given these assumptions, lateral flow rates beneath the disposal cell were calculated to be 2.2 gpm for the upper-middle unit, and 1.6 gpm for the lower-middle unit (DOE, 1987). Further, assuming that the tailings seepage is divided equally into each unit, and the long-term steady state seepage rate through the tailings is 1 x 10^{-8} cm/s (0.029 gpm), the mixing ratio (tailings seepage to groundwater underflow) was calculated to be 0.0066 for the upper-middle unit and 0.0091 for the lower-middle unit. Assuming a saturated infiltration barrier for steady state conditions, the mixing ratios would be 0.066 and 0.091, respectively. The dilution of the tailings seepage by groundwater underflow is proportional to these mixing ratios.

Tailings seepage from the proposed disposal cell was mixed with groundwater in the Cedar Mountain Formation beneath the cell by using the following mixing formula;

$$C_r Q_r = C_t Q_t + C_u Q_u$$

where

C_r = Resulting concentration of water quality constituent beneath the disposal cell (mg/l).

Q_r = Resulting flow rate beneath the disposal cell; equal to tailings seepage rate plus groundwater underflow (gpm).

2 b) Regarding ponding calculations, please see the attached note. The issue of seepage accumulation in the trenches has not been previously addressed. The minimum observed saturated conductivity of the bedrock is 7*10**-5 cm/sec, 700 times the maximum infiltration rate. We therefore do not consider accumulations of seepage above this unit to be possible.

A trench formed by the intersection of a partially below-grade cover with the edge of the bedrock excavation might allow water to pond along the edge of the cell. This note provides an estimate of the maximum amount of ponding expected with the current proposed design, and the implications for infiltration.

Figure 1 shows a section through the edge of the proposed cell and the adjacent host material. Water will be shed from the top of the cell through the bedding material and riprap. All infiltration is expected to penetrate the common fill where it is present, rather than drain laterally through the upper bedding layer. Infiltration reaching the lower bedding layer will either penetrate the clay cover or flow through the bedding to the bedrock contact. Runoff reaching the bedrock will accumulate until the saturated area of the rock and the driving force of water ponded in the trench produce discharge balancing the rate of runoff from the pile.

Beyond the edge of the radon barrier, rainfall infiltration will be limited by the permeability of the bedrock. The minimum observed permeability for this unit is 7×10^{-5} cm/sec or 2000 cm/year. Since this conductivity far exceeds annual rainfall, the bedrock will never become saturated in this area. Any off-pile recharge within the trench will infiltrate the bedrock rather than flowing downslope to the point of contact with the barrier. Ponding in the trench, if it occurs, will therefore results from water shed from the cell only.

To estimate the maximum amount of runoff from the cell, the following assumptions were made:

(1) The annual rainfall of 15 cm/year recharges the lower or common bedding layer over the entire surface of the pile, both above and below grade.

(2) No evaporation takes place.

(3) 10^{-7} cm/sec or 3 cm/year infiltrates through the radon cap, leaving a net excess recharge of 12 cm/year shed by the pile.

Because the radon cap must remain saturated for any runoff to occur, 12 cm/year represents the maximum flux rate to be disposed in the trench.

The total pile area is:

$$A = (440 \text{ ft})^2 = 1.8 \times 10^8 \text{ cm}^2$$

so that the maximum volume of runoff is

$$Q_{max} = (12 \text{ cm/year}) \times (1.8 \times \text{cm}^2) = 2.2 \times 10^9 \text{ cm}^3/\text{year}$$
$$= 68 \text{ cm}^3/\text{sec}$$

This runoff will create a ring of infiltration surrounding the pile (see Figure 2). Should ponding occur, the minimum infiltration rate will be the lower bound on bedrock permeability acting under a minimum gradient of 1:

$$q_{min} = 7 \times 10^{-5} \text{ cm/sec}$$

Note that this rate does not include the additional driving force created by ponding, and so underestimates the capacity of the trench to drain.

The area over which this infiltration occurs will be governed by the circumference of the pile (C), the width of the ponded zone D max, and the proportion of the ponded area in contact with the bedrock. The fraction of the ponded area allowing infiltration depends on the packing of the bedding material against the bedrock. Infiltration would enter the bedrock through the open pore spaces, and expand into regions blocked by grains of bedding material. We therefore expect the bedrock immediately below the contact area to be completely saturated, giving an effective-to-ponded infiltration area ratio near 1. As a conservative estimate, we assumed that the infiltration area will be limited to the open pore space area in the bedding material at the contact, giving an effective-to-ponded area ratio equal to the bedding layer porosity of .25. The effective infiltration area is approximately

$$A' = CDn = 4 \times (440 \text{ ft.}) \times D_{max} \times (.25) = 440 \text{ ft.} \times D_{max}$$
$$= 1.3 \times 10^{4} \text{ cm} \times D_{max}$$

The infiltration through the periphery must equal the maximum runoff rate:

$$Q_{max} = A' \times q_{min}$$

or

$$68 \text{ cm}^3/\text{sec} = 1.3 \times 10^{4} \text{cm} \times D_{max} \times 7 \times 10^{-5} \text{ cm/sec}$$

$$\Rightarrow D_{max} = 75 \text{ cm}$$

With a 2:1 excavation sideslope, this infiltration zone would produce a maximum ponding depth of 37 cm at the contact of the radon barrier with the bedrock. Current simulations of the proposed design predict a ponding height of 16 cm in the bedding layer. The maximum additional ponding in the trenches would increase vertical gradients through the barrier, and therefore infiltration around the edge of the cell. With the current 5:1 cover sideslope and a bedding thickness of .5 ft., this additional ponding would occur in a 100 cm (3.6 feet) skirt surrounding the cell (see Figure 3). The fraction of the cell area affected by this ponding is then:

$$f = C \times D'/A = (440 \text{ ft}) \times (3.6 \text{ ft})/(440 \text{ ft})^2 = 0.8\%$$

The maximum additional ponding of 37 cm over the 30 cm radon barrier will not increase infiltration by more than 50% over the modeled infiltration rate, which predicts 16 cm of ponding. The ponding height will decrease toward the center of the pile, producing an average exceedence over D' lower than 50%. Since the affected area is small compared to the total cell area, we expect insignificant impact on the overall percolation rate.

Assuming that the average observed bedrock conductivity of 1.6_{-4} ft/day is representative, the minimum infiltration rate will be 6×10^{-4} cm/sec, providing an extent of ponding of

$$D = 68 \text{ cm}^3/\text{sec} \; / \; (1.3 \times 10^4 \text{ cm}) \times (6 \times 10^{-4} \text{ cm/sec}) = 9 \text{ cm}$$

with a corresponding depth of ponding of 4.5 cm, less than that calculated in the simulations of infiltration through the cell. This result implies that the bedrock would be able to accept more water under a unit gradient than the bedding layer could deliver under a gradient of 20%.

In summary, we expect ponding in the sub-surface trench to increase infiltration by a maximum of 50% over a maximum of 0.8% of the pile, or 0.4% overall. This calculated increase is likely to be too large because of the following conservative assumptions:

(1) Neglect of evaporative losses;

(2) Neglect of the effect of bedding layer ponding on radon barrier infiltration, and consequent over estimation of runoff;

(3) Neglect of contribution of ponding in the trench to bedrock infiltration;

(4) Use of the minimum observed bedrock conductivity as representative of the conductivity along the trench;

(5) The assumption that the effective draining area is limited by bedding-layer porosity;

(6) The assumption that the maximum ponding occurs over the entire affected area of the radon barrier;

(7) Inclusion of innocuous infiltration through the radon barrier, where it abuts the bedrock, as a contribution to leachate generation.

MORRISON KNUDSEN ENGINEERS

Project _____ Contract No. _____ Sheet _____
Feature _____ Designed _____ File No. _____
Item _____ Checked _____ Date _____ Date _____

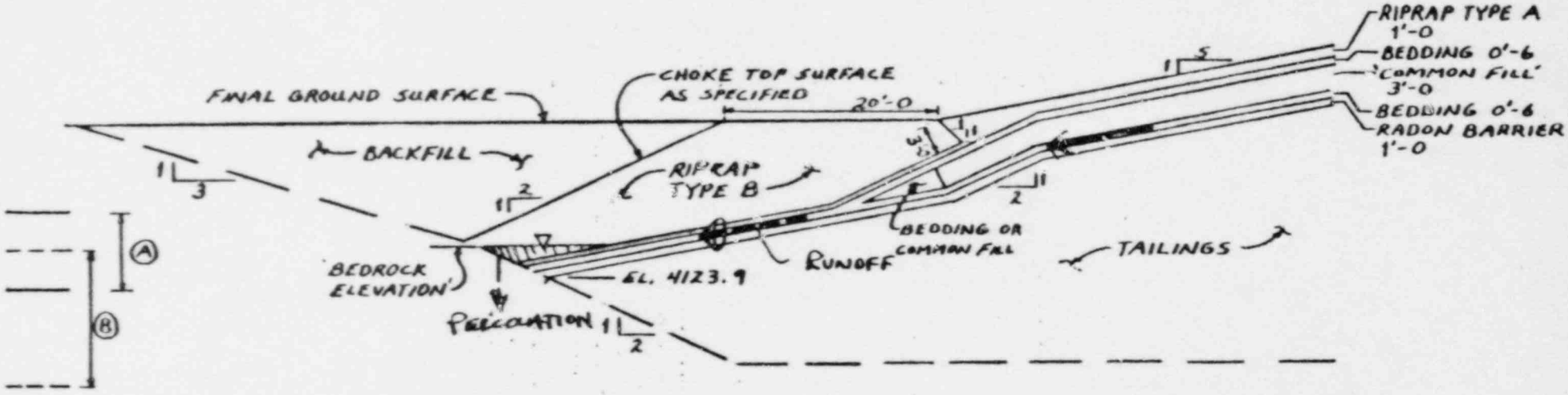

Ⓐ = ELEVATION OF BEDROCK IN VICINITY OF EMBANKMENT (EXCLUDING SE SIDE).

Ⓑ = APPROX. ELEVATION OF TOP SURFACE OF CEDAR MT. FORMATION, SHALE, CLAYSTONE, AND/OR CLAY (EXCLUDING SE SIDE)

SCALE FEET
0 20

UMTRA GREEN RIVER SITE

RIPRAP TOE PROTECTION DETAIL

(FOR STUDY PURPOSES ONLY)

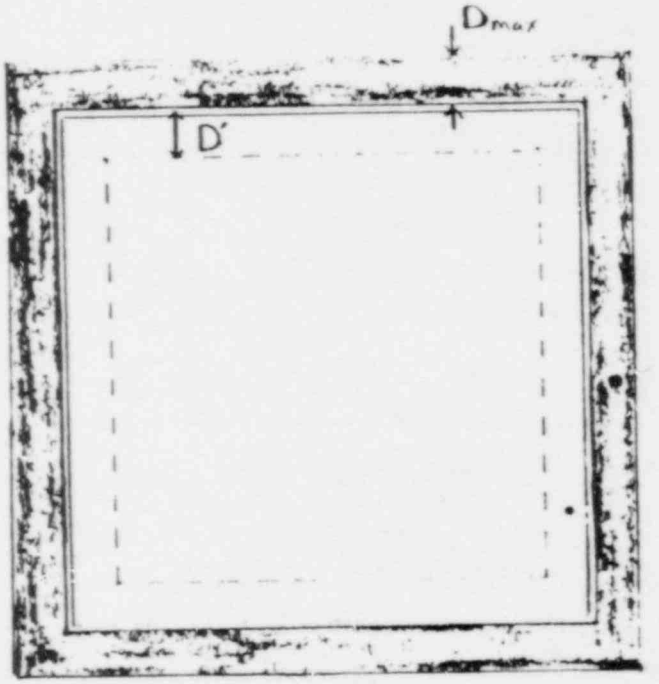

—— Cell Boundary

D_{max} Lateral Extent of Bedrock Saturation

D' Lateral Extent of Ponding over the Cell

Area of Ponding over Bedrock

Area of Ponding over Tailings

NOTE: Not to Scale

Figure 2 - Schematic Diagram of Areas Affected by Ponding in the Trench

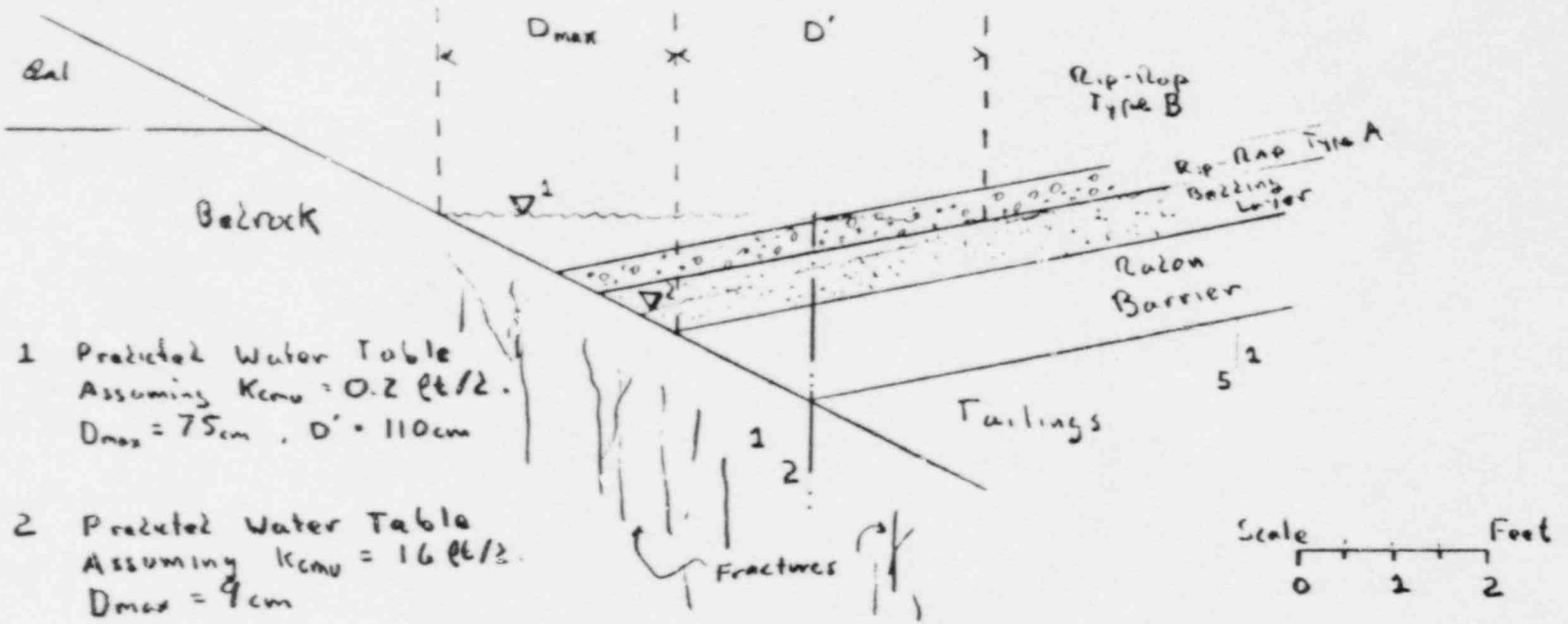

Figure 3 - Predicted Conditions in the Trench Created by the Proposed Design

Dispersion

Nitrate dispersion was modeled using the Domenico and Robbins (1985) two-dimensional dispersion model. Detailed input and results are on file at the UMTRA Project Office, Albuquerque, New Mexico. (c)

Modeling input and results are summarized in Table D.5.26. Nitrate concentration will disperse to a background level (currently beneath the proposed disposal site) of 99 mg/l at a distance of 435 feet downgradient of the mixing zone in the lower-middle unit. Since the mixing zone for the lower-middle unit is beneath the northern half of the disposal cell (see the section entitled "Mixing and dilution"), 435 feet downgradient of the mixing zone is approximately the downgradient toe of the disposal cell. This analysis is assuming the tailing seepage is equal to 0.029 gpm (seepage flux of 10^{-8} cm/s). This analysis also assumes no geochemical attenuation. Dispersion estimates (assuming no geochemical attenuation) were also made for a tailings seepage rate of 0.29 gpm (seepage flux of 10^{-7} cm/s) for the lower-middle unit; tailing seepage rates of 0.029 and 0.29 gpm for the upper-middle unit; and distances to disperse to the local background level as well as the proposed EPA MCL for nitrate (44 mg/l as NO_3).

Uranium and gross alpha dispersion was not modeled because of the high resultant concentrations of these constituents estimated by mixing calculations. The dispersion modeling would not be helpful in making a realistic estimate of the fate of the uranium and gross alpha. Geochemical attenuation is expected to be an important factor in removing these contaminants from the groundwater downgradient of the disposal cell. If uranium concentrations are not lowered to local background levels or the proposed EPA MCL of 0.044 mg/l within 600 ~~500~~ feet downgradient of the disposal site, the fate of the uranium plume will be the same as the fate of the uranium plume currently in the upper-middle shale unit. Any uranium in the lower-middle sandstone unit would also disperse, and since the lower-middle unit intertongues with the upper-middle unit west (downgradient) of the present tailings pile (see Figures D.5.2 and D.5.3), the fate of any uranium (and gross alpha) contamination in the lower-middle unit would likely be similar to that of the upper-middle unit.

Geochemial attenuation

Concentrations of arsenic, barium, lead, mercury, and silver within tailings pore fluid and the Cedar Mountain Formation aquifer are below proposed EPA maximum concentration limits (MCL); therefore, these contaminants are not addressed. Concentrations of cadmium, chromium, nitrate, selenium, and uranium, however, exceed EPA MCLs within tailings pore fluid

2 c) The enclosed summary sheet show the input parameters for the Domenico-Robbins dispersion model, the calculation of the ratio of maximum nitrate concentrations to the anticipated source concentrations, and the resulting measures of the MCL isopleth: downgradient distance from the source (the tailings) and half-width of the plume at half this distance.

The article published in "Groundwater" describing the solution used in these calculations has also been included along with a listing of the programs implementing this solution. The first program iteratively finds the downgradient distance at which the calculated concentration equals a user-specified value. The second program uses the same iterative scheme to find the off-gradient distance to the point of specified concentration.

In application to the Green River site, as at other sites where vertical dispersion is limited by stratigraphy or [illegible] undetermined, vertical dispersion coefficients were set to an extremely small value (7.8*10**-7 ft) in order to eliminate dispersion in the z-direction.

Because the source concentrations [illegible] are expected to exceed the MCL [illegible] geochemical attenuation is not expected to [illegible] the [illegible] distance [illegible]

JACOBS ENGINEERING

DATE Feb 10, 1988 SUBJECT Summary of Domenico-Robbins Dispersion Calculations SHEET NO 1/1

BY Welch CHKD. JOB NO.

	Lower-middle unit	Upper-middle unit
Regional background conc.	1 mg/l	4 mg/l
Local background conc.	99 mg/l	85 mg/l
Nitrate MCL	44 mg/l	44 mg/l
Source concentration	134 - 297 mg/l	100 - 223 mg/l
Velocity	40 ft/yr	74 ft/yr
α_L, α_T	100 ft	100 ft
Source width	700 ft	830 ft
Source thickness	20 ft	30 ft

Lower-middle unit

Percolation rate [cm/sec]

Target conc. [mg/l] \ Source conc [mg/l]	10^{-8} 134	10^{-7} 297
44	.32	.15
99	.74	.33

Upper-middle unit

Percolation rate [cm/sec]

Target conc. [mg/l] \ Source conc [mg/l]	10^{-8} 100	10^{-7} 223
44	.42	.18
85	.84	.37

$$C/C_0 = \frac{\text{Target} - \text{Reg'l background}}{\text{Source} - \text{Reg'l background}}$$

Lower-middle unit

Percolation rate [cm/sec]

Target conc. [mg/l] \ Source conc. [mg/l]	10^{-8} 134	10^{-7} 297
44	1740	4250
99	735	1670

Upper-middle unit

Percolation rate [cm/sec]

Target conc. [mg/l] \ Source conc. [mg/l]	10^{-8} 100	10^{-7} 223
44	2430	7900
85	440	2990

O^* - distance in feet to disperse to target concentration in 1000 years

Lower-middle unit

Percolation rate [cm/sec]

Target conc [mg/l] \ Source conc. [mg/l]	10^{-8} 134	10^{-7} 297
44	510	890
99	210	500

Upper-middle unit

Percolation rate [cm/sec]

Target conc. [mg/l] \ Source conc. [mg/l]	10^{-8} 100	10^{-7} 223
44	460	950
85	205	530

W^* - plume half-width in feet at $\frac{1}{2} O^*$

A New Method of Contaminant Plume Analysis

by P. A. Domenico and G. A. Robbins[a]

ABSTRACT

This paper develops an analytical expression for contaminant transport from a finite source in a continuous flow regime. The model requires some numerical integration and its degree of accuracy for near-field problems depends on discretization procedures applied to the source boundary. A second model for a continuous source is developed by extending a well-known pulse model. This second model is particularly useful in that it permits the determination of several potential unknowns directly from a concentration distribution. These include the source concentration, source dimensions, the position of the center of mass which is the product of the seepage velocity and the time since the contaminant first entered the ground water, and up to three dispersivities for a three-dimensional problem. As a demonstration of its utility, this second model is applied with reasonable success to a well-defined field condition. A comparison of the two models indicates that, except for minor differences in the very near field, the results from each are virtually identical.

INTRODUCTION

The use of models in problems of contaminant transport is rapidly increasing in response to the need to measure, monitor, and apply predictive approaches to contaminant plumes of various size and shape. An impressive array of numerical and analytical models is available, both for instantaneous pulses and for continuous sources. Many of the analytical models are quite sophisticated and generally require some numerical integration (Prakash, 1982). In the more simple closed form category for instantaneous pulses are the models of Baetsle (1969) and Hunt (1978). For continuous source problems, the hydrogeologist may draw on the relatively simple two-dimensional model of Wilson and Miller (1978) or the three-dimensional solution of Hunt (1978). Unfortunately, these latter models require that the source be treated as a point and, consequently, are only applicable to the far field. Whatever model is contemplated, one of the more formidable problems in contaminant transport is the difficulty in assessing the important parameters and coefficients, including source concentration and dimensions, seepage velocity, time since the contaminant first entered the ground water, and up to three dispersivities for a three-dimensional problem. This problem is addressed in this paper with the development of two continuous finite source models. The most rigorous of these models requires some numerical integration, and does not offer any special advantages over other models in that it offers no new methods by which to determine these parameters and coefficients. A second model, however, appears to be useful in these determinations. A comparative analysis is performed to assess their mutual reliability in field situations.

MATHEMATICAL CONSIDERATIONS

The dispersion-convection equation is of the form

$$\partial C/\partial t + v\partial C/\partial x - D_x\partial^2 C/\partial x^2 - D_y\partial^2 C/\partial y^2 - D_z\partial^2 C/\partial z^2 = 0 \qquad (1)$$

where C is concentration in mass per unit volume of water; D_x, D_y, D_z are the principal values of the dispersion tensor; t is time; x, y, z represent Cartesian coordinates which are presumed to coincide with the principal directions of the dispersion tensor; and v is the ground-water seepage velocity. For the continuous finite source, the source condition is described by

$$F(x,y,z,t) = M \quad \text{for } x = 0,\ -Y < y < Y,\ -Z < z < Z,\ \text{all } t \qquad (2)$$

$$= 0 \quad \text{otherwise}$$

where F represents the source term of the contaminants; Y and Z are the source dimensions in y and

---

[a]Department of Geology, Texas A&M University, College Station, Texas 77843.

Received September 1984, revised November 1984, accepted December 1984.

Discussion open until January 1, 1986.

z, respectively; and M = the strength of the source, $mL^{-2}t^{-1}$. This describes a continuous injection mt^{-1} at x = 0 over the area $-Y < y < Y$, $-Z < z < Z$.

The solution to equation (1) with equation (2) is

$$C(x,y,z,t) = \int_0^t \int_{R_e} \int \{M/8[\pi^3 D_x D_y D_z (t-t')^3]^{1/2}\}$$

$$\exp\{-[x - x' - v(t-t')]^2/4D_x(t-t') -$$

$$(y-y')^2/4D_y(t-t') - (z-z')^2/4D_z(t-t')\} \cdot$$

$$dx', dy', dz', dt' \qquad (3)$$

where R_e indicates the triple integration over the region which x', y', and z' are extended. Integrating over dx' yields

$$C(x,y,z,t) = \int_0^t \{M dt'/8[\pi^3 D_x D_y D_z (t-t')^3]^{1/2}\}$$

$$\exp - \{[x - v(t-t')]^2/4D_x(t-t')\} \int_{-Y}^{Y} \int_{-Z}^{Z} dy'\, dz'$$

$$\exp\{[-(y-y')^2/4D_y(t-t') - (z-z')^2/4D_z(t-t')]\}$$

$$\ldots\ldots\ldots (4)$$

To make further progress with the finite source expression of equation (4), it is assumed that the order of integration can be interchanged, i.e., the operations involving dt' will be done before those involving dy' and dz'. In this case, equation (4) becomes

$$C(x,y,z,t) = \int_{-Y}^{Y} \int_{-Z}^{Z} dy'\, dz' \int_0^t$$

$$\{M\, dt'/8[\pi^3 D_x D_y D_z (t-t')^3]^{1/2}\}$$

$$\exp\{-[x - v(t-t')]^2/4D_x(t-t') -$$

$$(y-y')^2/4D_y(t-t') - (z-z')^2/4D_z(t-t')\}. \qquad (5)$$

In the form, the integral over dt' has already been presented by Hunt (1978) for a continuous point source. Incorporating Hunt's (1978) results in equation (5) yields

$$C(x,y,z,t) = \int_{-Y}^{Y} \int_{-Z}^{Z} dy'\, dz' \cdot$$

$$[M \exp(xv/2D_x)/8\pi R(D_y D_z)^{1/2}] \cdot$$

$$[\exp(-Rv/2D_x)\,\mathrm{erfc}\{(R - vt)/2(D_x t)^{1/2}\} +$$

$$\exp(Rv/2D_x)\,\mathrm{erfc}\{(R + vt)/2(D_x t)^{1/2}\}] \qquad (6)$$

where

$$R = [x^2 + (y-y')^2 D_x/D_y + (z-z')^2 D_x/D_z]^{1/2} \qquad (7)$$

The quantity R differs from the R in Hunt (1978) in that y and z are replaced by y - y' and z - z'. For a point source, y' = z' = 0 and the integrals over dy' and dz' would be dropped, resulting in Hunt's (1978) three-dimensional continuous point source solution.

The steady-state form of equation (6) is expressed

$$C'(x,y,z,\infty) = \int_{-Y}^{Y} \int_{-Z}^{Z} dy'\, dz' \cdot$$

$$[M/4\pi R(D_y D_z)^{1/2}] \exp[(x - R)v/2D_x] \qquad (8)$$

where C' indicates the steady-state concentration.

Given the complexity of equation (6), deriving a closed form solution which includes the temporal variations is virtually ruled out. The integrals in equation (8) can likely be worked out for a special type of elliptic source region, or for a circle, but these will be of limited value in real contamination problems. In spite of this difficulty, equation (6) is quite interesting in that it demonstrates how a closed form continuous point source solution is incorporated within a complex finite source solution. Hence, from a practical point of view, all that is required is the replacement of a continuous source region of any shape or size by an array of discrete points for which the solution is already known. The field distribution of concentration can then be determined by superposition. This is demonstrated in the following section.

SUPERPOSITION MODEL

As expressed by equation (6), the solution to the finite source problem is the integration of the point source model of Hunt (1978) over the area of the finite source. The numerical integration entails the following. First, the finite source is divided into a grid of node centered cells having equal area with a symmetrical distribution about the center point of the finite source. The volumetric flow rate through each cell is then equal to the total flow rate through the source divided by the number of cells. Second, the point source model of Hunt (1978) is used to calculate the concentration at a point of interest resulting from flow through each node. This entails adjusting the spatial coordinates of the point of interest with respect to each node's position relative to the center of the source. That is, each point of interest where a concentration determination is required is associated with an x, y, and z coordinate with respect to the center node of the source, as well as x', y', and z' coordinates with respect to each node within the source. Third, the

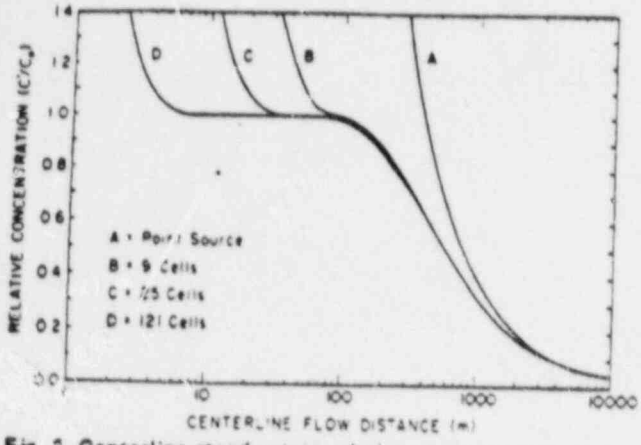

Fig. 1. Centerline steady-state relative concentration versus distance curves, for the superposition model.

calculated concentrations for all nodes are then summed. This approach can be applied to a source of any size or shape, and calculations are relatively straightforward and easily programmed for microcomputer analysis.

To illustrate the superposition model, a series of calculations were performed for a source having a square cross section. The source measured 5 × 5 m, the total source flow rate equals 250 $cm^3\ sec^{-1}$, the seepage velocity is taken as 1×10^{-3} cm sec^{-1}, the longitudinal dispersion coefficient equals 1×10^{-3} $cm^2\ sec^{-1}$, and the transverse coefficients in y and z are assumed equal and taken as 5×10^{-4} $cm^2\ sec^{-1}$.

Figure 1 illustrates centerline (x, 0, 0) steady-state concentration ratio (C'/C_o) versus distance curves where the source was divided into grids having 9, 25, and 121 cells. Here, C' is the maximum steady-state concentration and C_o is the source concentration. For comparative purposes, centerline concentrations are presented for the case where the source is treated as a single point with Hunt's (1978) model. As demonstrated on the figure, as the number of cells increase, the configuration of the concentration distribution takes on the shape of a more normal breakthrough curve, and the distance at which the source concentration is predicted approaches the actual source position. This effect is due to the boundary condition in Hunt's (1978) model such that as x approaches zero, the concentration approaches infinity. These characteristics are best explained by Hunt's (1978) point source centerline concentration at steady state

$$C'(x,0,0,\infty) = C_o Q/4\pi x (D_y D_z)^{1/2} \qquad (9)$$

where C_o is the source concentration mL^{-3}, and Q is the point source flow rate L^3t^{-1}. Setting the maximum concentration C' equal to the source concentration C_o, and determining the position at which this concentration occurs gives

$$x = Q/4\pi (D_y D_z)^{1/2} \qquad (10)$$

Hence, the distance at which the near-field concentration converges on C_o does not coincide with the position x = 0, but is directly proportional to the volumetric source rate Q. As the number of cells in the superposition model increase, the magnitude of Q decreases for each node, although the total source Q remains constant. For example on Figure 1, the 121-cell model predicts the source concentration at a distance of only 7 m from the source. As expected, finite and point source calculations converge in the far field (Figure 1).

EXTENDED PULSE APPROXIMATION

The superposition model given above is relatively straightforward and can be readily applied to well-defined plumes emitting from some finite continuous source. This model, along with all transport models, incorporates several potential unknowns, including the source concentration and dimensions, the seepage velocity, time since the contaminant entered the ground water, and three dispersion coefficients. In this sense it offers no special advantages over straightforward numerical or other analytical approaches to the finite source problem. Cleary (1978), for example, presents several analytical solutions, all of which require some numerical integration. In a practical sense, it is advantageous to have a much simpler but still reasonably equivalent approximation to this model which is better suited for direct determination of the pertinent coefficients and parameters. As the development of such a model will require some approximations, its ultimate test will rely on how close its performance matches the more rigorous superposition model. A first-order attempt at obtaining such a model requires an extension of the parallelepiped instantaneous pulse shown in Figure 2. This parallelepiped model is given by Hunt (1978), and is of the form

$$C(x,y,z,t) = (C_o/8)\{\mathrm{erf}[x - vt + (X/2)/2(D_x t)^{1/2}] - \mathrm{erf}[x - vt - (X/2)/2(D_x t)^{1/2}]\}$$
$$\{\mathrm{erf}[y + (Y/2)/2(D_y t)^{1/2}] - \mathrm{erf}[y - (Y/2)/2(D_y t)^{1/2}]\}$$
$$\{\mathrm{erf}[z + (Z/2)/2(D_z t)^{1/2}] - \mathrm{erf}[z - (Z/2)/2(D_z t)^{1/2}]\} \qquad (11)$$

where X, Y, and Z refer to the original source dimensions. This solution describes the convection

and dispersion of a substance deposited at time $t = 0$ in the region $-X/2 < x < X/2$, $-Y/2 < y < Y/2$, $-Z/2 < z < Z/2$, as shown in Figure 2. Clearly, in this solution, C_o approaches zero in the $x = 0$ plane as time gets large. For the continuous plane source of dimensions Y and Z [equation (5)], it is required that the concentration be maintained at C_o for all time in the $x = 0$ plane and, of course, be equal to zero at $x > 0$ for time equal to zero. This effect can be accomplished with the box of Figure 2 by extending the box to infinity in the minus x direction. Continuous mass flow from the $x = 0$ plane is then accomplished by the extended contaminant source. More commonly, the process is described by an infinite number of line sources resulting in an infinite number of elementary solutions which must be superposed, i.e., integrated from some x to infinity (Crank, 1979, p. 13). According to Crank (1979, p. 14), this is described as

$$C(x,t) = [C_o/2(\pi D_x t)^{1/2}] \int_x^\infty \exp(-\xi^2/4D_x t)\, d\xi$$

$$= [C_o/\pi^2] \int_{x/2(D_x t)^{1/2}}^\infty \exp(-\eta^2)\, d\eta \qquad (12)$$

where $\eta = \xi/2(D_x t)^{1/2}$. Equation (12) can be expressed by the simple complementary error function solution

$$C(x,t) = (C_o/2)\,\mathrm{erfc}\,[(x - vt)/2(D_x t)^{1/2}] \qquad (13)$$

which describes continuous mass flow from the $x = 0$ plane. Equation (13) is obtained exactly when X is extended to infinity in the first bracketed erf term in equation (11).

There still remains an accounting of the substance initially confined in the region $-Y/2 < y < Y/2$ and $-Z/2 < z < Z/2$. According to Crank (1979, p. 15) the integration here is from $y - Y/2$ to $y + Y/2$ and $z - Z/2$ to $z + Z/2$, instead of from x to infinity as in equation (12). This gives

$$C = (C_o/2)\,\mathrm{erf}\,[(y + Y/2)/2(D_y t)^{1/2}] - \mathrm{erf}\,[(y - Y/2)/2(D_y t)^{1/2}] \qquad (14\text{-}1)$$

$$C = (C_o/2)\,\mathrm{erf}\,[(z + Z/2)/2(D_z t)^{1/2}] - \mathrm{erf}\,[(z - Z/2)/2(D_z t)^{1/2}]\,. \qquad (14\text{-}2)$$

The product of these three integral solutions [equations (13) and (14)] describes a semi-infinite contaminated parcel which moves in the positive x direction with a one-dimensional velocity but which continually expands in size in directions transverse to x throughout the whole domain of x, i.e., in the positive and negative regions. This is because time t in the transverse spreading terms of equation (14) is interpreted as running time. Reinterpreting this time as x/v for a moving coordinate system, as is common in all transverse spreading models (Bruch and Street, 1967; Ogata, 1970; Domenico and Palciauskas, 1982), has the effect of maintaining the original source dimensions at $x = 0$ so that the condition $C \cong C_o$ is maintained at $x = 0$ for $t > 0$. Making this substitution and collecting equations (13) and (14) gives

$$C(x,y,z,t) = (C_o/8)\,\mathrm{erfc}\,[(x - vt)/2(D_x t)^{1/2}]$$
$$\{\mathrm{erf}\,[(y+Y/2)/2(D_y x/v)^{1/2}] - \mathrm{erf}\,[(y-Y/2)/2(D_y x/v)^{1/2}]\}$$
$$\{\mathrm{erf}\,[(z+Z/2)/2(D_z x/v)^{1/2}] - \mathrm{erf}\,[(z-Z/2)/2(D_z x/v)^{1/2}]\} \qquad (15)$$

Equation (15) is given as the extended pulse approximation to the continuous finite source problem. It describes a semi-infinite contaminated parcel which moves with a one-dimensional velocity in the positive x direction. It is noted that at the source boundary $x = y = z = 0$ for time greater than zero, the product of the error functions equals four, and the argument of the complementary error function takes on a negative number. The value of the complementary error function ranges from plus two to zero, taking on the former value for arguments equal to negative infinity. However, in a practical sense, the maximum value of two is approximated for very small negative values of the argument. For example, when the argument $[(x - vt)/2(D_x t)^{1/2}]$ equals negative two, the complementary error function equals 1.99. Thus, in a practical sense, the source concentration is maintained at or near C_o for times greater than zero.

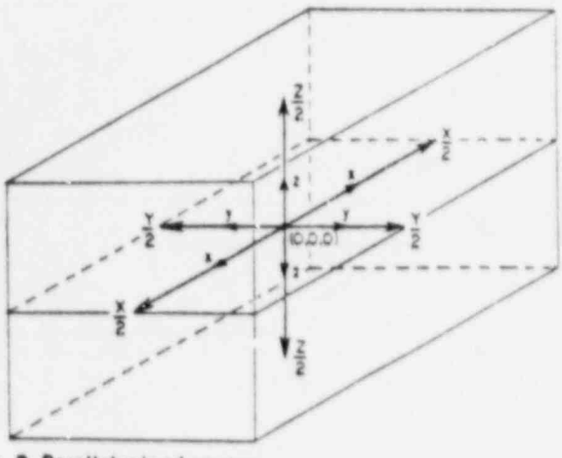

Fig. 2. Parallelepiped source.

Two forms of equation (15) are of interest. The first is for the centerline concentration (x,0,0,t)

$$C(x,0,0,t) = (C_o/2)\,\mathrm{erfc}\,[(x - vt)/2(D_x t)^{1/2}]$$
$$\mathrm{erf}\,[Y/4(D_y x/v)^{1/2}]\,\mathrm{erf}\,[Z/4(D_z x/v)^{1/2}] \quad (16)$$

The boundary condition at x = 0 is more apparent with this expression. At x = 0, the error function terms go to unity and for time greater than zero, the complementary error function rapidly approaches two. The second expression is for the steady-state concentration (i.e., the maximum at x,0,0) along the centerline, which is obtained at all $x << vt$

$$C' = C_o\,\mathrm{erf}\,[Y/4(D_y x/v)^{1/2}]\,\mathrm{erf}\,[Z/4(D_z x/v)^{1/2}] \quad (17)$$

where C' is the steady-state concentration. It is noted further that for Y and Z considerably larger than $4(D_y x/v)^{1/2}$ and $4(D_z x/v)^{1/2}$, respectively, the centerline concentration can approach the initial concentration throughout some distance x.

Equation (15) is quite versatile in describing different spreading geometries. As written, equation (15) applies to the spreading geometry schematically illustrated in Figure 3(b), which corresponds to the numerical integration of Hunt's (1978) point source model [equation (6)]. If the upper surface of a contaminant plume coincides with the water table so as to provide only downward z spreading, as illustrated in Figure 3(a), the quantities Z/2 in equation (15) are replaced by Z. This problem can be viewed as a contaminated parcel bounded at the top, z = 0, by a zero flux boundary, with transverse spreading in all y, but in only one vertical direction. In this form, equation (15) is analogous to a transverse dispersion solution presented by Domenico and Palciauskas (1982) with the exception that this current form has provisions for longitudinal dispersion. If contaminant spreading in z is restricted, as illustrated in Figure 3(c), equation (15) would be modified by changing $C_o/8$ to $C_o/4$ and dropping the error functions containing the Z terms. In this form, the model corresponds to a numerical integration of the Wilson and Miller (1978) line source model.

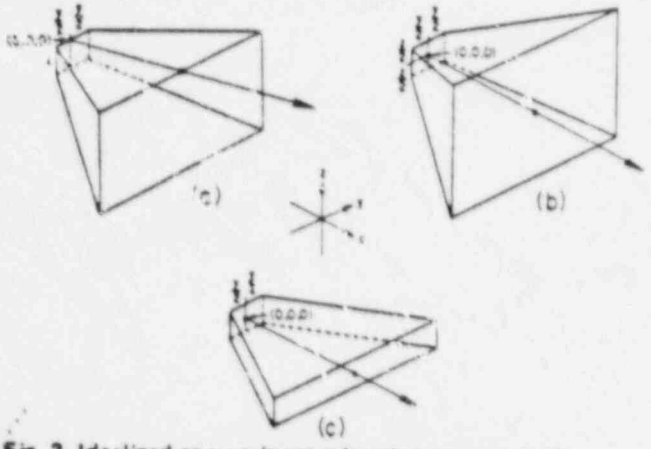

Fig. 3. Idealized contaminant migration geometries for various transverse spreading directions.

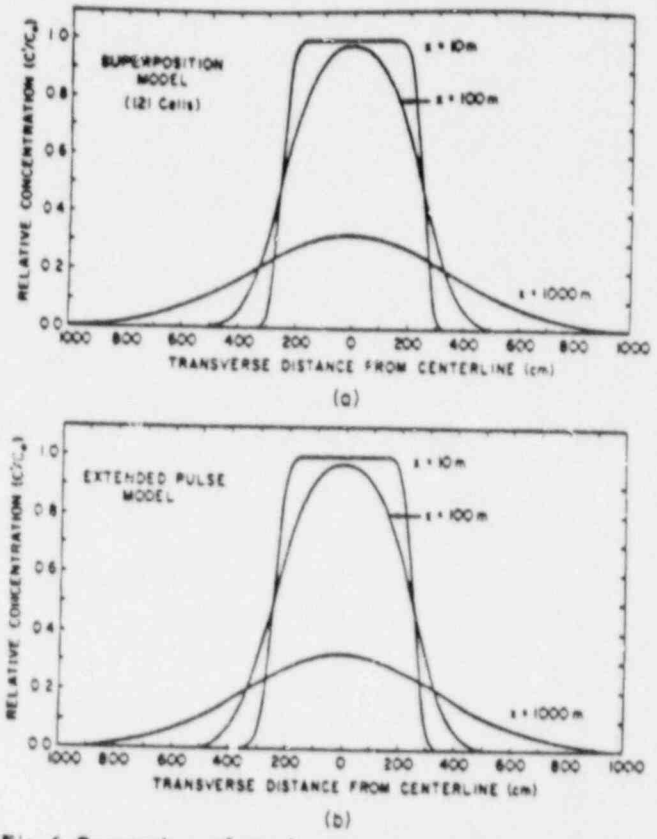

Fig. 4. Comparison of steady-state transverse concentration profiles with identical coefficients for (a) the superposition model, and (b) the extended pulse model.

Figure 4 shows steady-state transverse profiles for the extended pulse and the 121-cell superposition model as generated from the same data employed in Figure 1. At about two source sizes (10 m) and beyond, the extended pulse matches the 121-cell superposition result.

The results of an additional check are demonstrated in Figure 5 for a field size plume. Here, the same coefficients and parameters are employed in both the superposition and extended models for an assumed spreading geometry as given in Figure 3(b). The coefficients and parameters are as follows: $D_x = 1.06$ cm^2 sec^{-1}, $D_y = 0.21$ cm^2 sec^{-1}, $D_z = 0.00016$ cm^2 sec^{-1}, Y = 240 m, Z = 5 m, the seepage velocity $v = 2.49 \times 10^{-4}$ cm sec^{-1}, $C_o = 850$ mg/l, time t is taken as 14 years, and the source flow rate Q is obtained from information on velocity and source size, or 3×10^3 cm^3 sec^{-1}. Thus, for this identical set of parameters and

coefficients, the plumes should be identical provided the extended pulse is a reasonable approximation for the finite source problem, as described more rigorously by the superposition model. The superposition result is shown in Figure 5 (a) and the extended pulse in Figure 5 (b). Comparing the results of the two calculations, it is noted that within one source dimension (Y), the concentrations differ by less than 10 percent. At a distance within two source dimensions, the concentrations differ by less than two percent. Beyond two source dimensions, the results are virtually identical.

A METHOD OF CONTAMINANT PLUME ANALYSIS

In this section, a calibration method for determining the pertinent coefficients and parameters using the extended pulse model is discussed. The procedure employed is exactly the same procedure that has been used for decades in the application of well hydraulics—that is, the matching of real response data with an idealized mathematical model that presumably describes that response. As with well hydraulics, deviations from the ideal behavior are to be expected, and

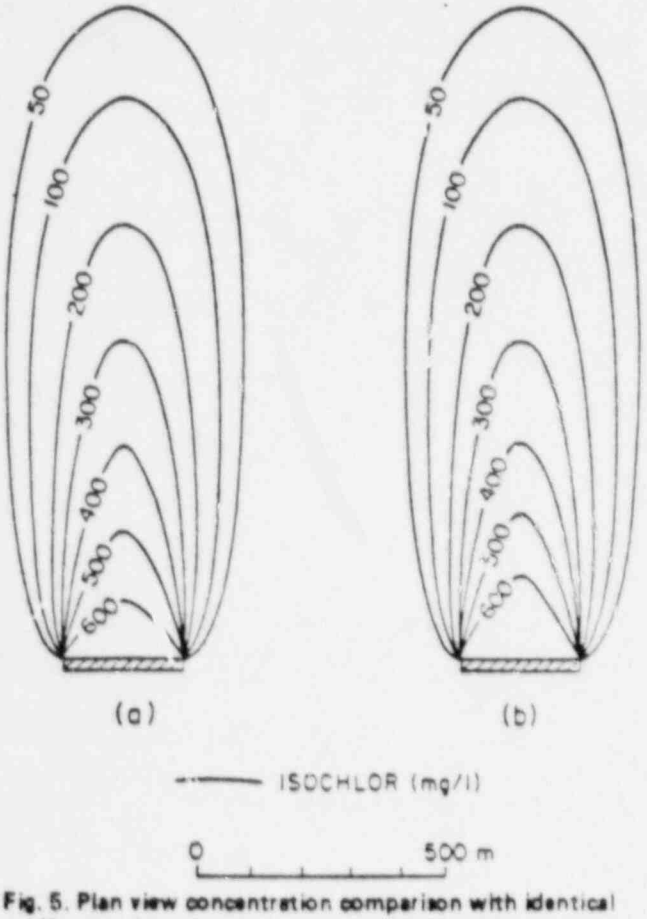

Fig. 5. Plan view concentration comparison with identical coefficients for (a) superposition model and (b) extended pulse model.

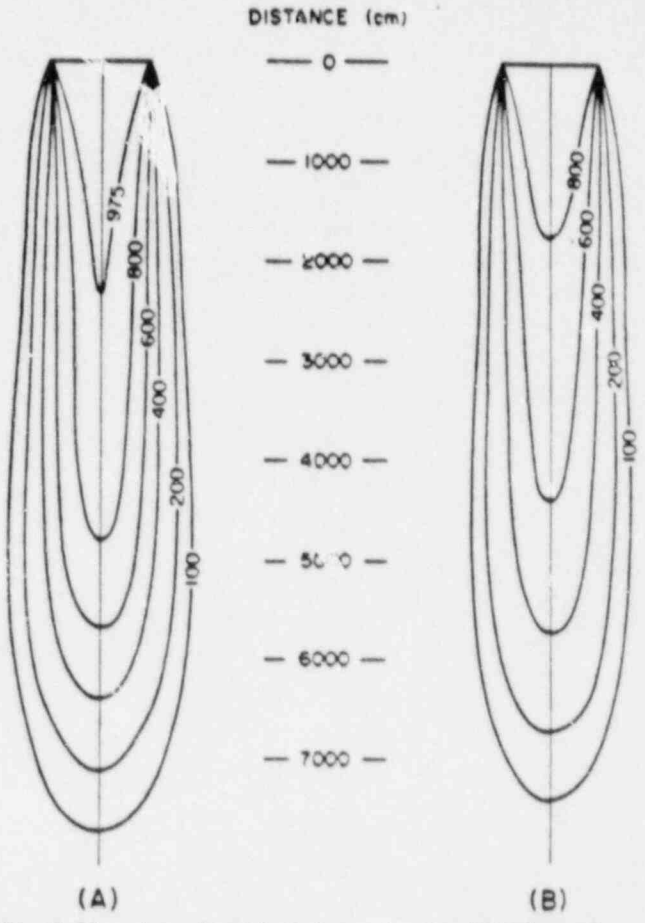

Fig. 6. Plan view of an ideal plume showing (A) plane of maximum concentrations and (b) plane of lower concentrations near the base of the source.

provide a measure of how much the real system departs from the ideal one. For this case, real response data are provided by some observed concentration distribution in space whereas the mathematical model of that response is provided by equation (15).

Figure 6 gives two plan views of an ideal plume generated with equation (15) for the case where the upper surface of the plume coincides with the water table [Figure 3(a)]. Figure 6(A) gives the concentration distribution $C(x,y,0,t)$ at the water table, which is the plane of maximum concentration, whereas Figure 6(B) gives the concentration $C(x,y,z,t)$ where z is taken at 50 cm above the base of the source. Due to this spreading geometry, the lowermost plane [Figure 6(B)] contains lower concentrations than the uppermost plane [Figure 6(A)]. For this idealized plume, the dispersivities α were assumed to be about tracer scale in magnitude, where α_x = 100 cm, α_y = 10 cm, and α_z = 1 cm. In addition, the seepage velocity was assumed to be 10^{-4} cm/sec, the source dimensions Y and Z were taken as 1,000 and 500 cm, respectively, the source concentration was

taken at 1,000 mg/l, and the time of interest is two years.

From the form of equation (15) appropriate to this problem, the following ratio for two concentrations may be derived for two points common to any single horizontal plane in the three-dimensional plume

$$C(x_1,y_1,z_1,t_1)/C(x_1,y_2,z_1,t_1) = \{\text{erf}[(y_1 + Y/2)/2(\alpha_y x_1)^{1/2}] - \text{erf}[(y_1 - Y/2)/2(\alpha_y x_1)^{1/2}]\} \div \{\text{erf}[(y_2 + Y/2)/2(\alpha_y x_1)^{1/2}] - \text{erf}[(y_2 - Y/2)/2(\alpha_y x_1)^{1/2}]\} \quad (18)$$

where $y_1 \neq y_2$. For a field application, where the concentration ratio in equation (18) is known from measurement, an iteration routine gives rather complete information on the relationship between α_y and Y. The results of this iteration are shown in Figure 7(A) for various concentration ratios taken off the $z = 0$ plane [Figure 6(A)]. For the close-in points ($x = 4{,}000$ cm), the transverse coefficient is very sensitive to the source dimension. The concentration ratio of equation (18) for these two particular points can be satisfied with any combination of Y and α_y taken off this curve. For the furthest points ($x = 8{,}000$ cm), the transverse coefficient is less sensitive to the source dimension Y, which is fully expected for points distant from some finite source. The concentration ratio of equation (18) for these particular points can be satisfied with any combination of Y and α_y taken off this curve. One property of the ideal plume is that those points closest to the source have the largest intercept on the α axis. The most important property is that the common point of intersection for the three curves of Figure 7(A) provides the unique source dimension Y and transverse dispersivity α_y for the total field distribution, in this case 1,000 cm and 10 cm, respectively. It may be noted further that the use of a source dimension smaller than the actual results in a scaling upward of dispersivity, while use of a larger source dimension results in downward scaling.

A similar routine can be established for α_z and the source dimension Z by considering the concentrations $C(x_1,y_1,z_1,t_1)$ and $C(x_1,y_1,z_2,t_1)$. Figure 7(B) gives the relationship between the transverse coefficient α_z and the source dimension Z for the ideal plume of Figure 6, with the point of intersection denoting the unique values. If $C(x_1,y_1,z_2,t_1)$ is unknown, as in the case of mapping a plume in the $(x,y,0)$ plane, an iteration procedure can still be followed by taking the ratio of two steady-state concentrations in the $(x,y,0)$ plane. For this model, the steady-state concentration is described

$$C'(x,y,0) = (C_o/2)\{\text{erf}[(y + Y/2)/2(\alpha_y x)^{1/2}] - \text{erf}[y - Y/2)/2(\alpha_y x)^{1/2}]\}\{\text{erf}[Z/2(\alpha_z x)^{1/2}]\} \quad (19)$$

where C' is the steady-state (maximum) concentration. If two steady-state concentrations are selected along the centerline $(x,0,0)$, the ratio of the concentrations can be expressed

$$C'(x,0,0)/C'(x_2,0,0) = \{\text{erf}[Y/4(\alpha_y x_1)^{1/2}]\,\text{erf}[Z/2(\alpha_z x_1)^{1/2}]\} \div \{\text{erf}[Y/4(\alpha_y x_2)^{1/2}]\,\text{erf}[Z/2(\alpha_z x_2)^{1/2}]\} \quad (20)$$

which is readily iterated in terms of α_z and Z.

The procedures developed above would appear to be quite efficient in obtaining the transverse coefficients and appropriate source dimensions from field distributions of contaminants. It is noted that these parameters are obtained independent of source concentration, seepage velocity, longitudinal dispersivity, and time. This methodology can now be extended to determine the remaining unknowns in the problem. For the plume geometry under consideration, the steady-state centerline solution is expressed

$$C'(x,0,0) = C_o\,\text{erf}[Y/4(\alpha_y x)^{1/2}]\,\text{erf}[Z/2(\alpha_z x)^{1/2}] \quad (21)$$

if a steady-state concentration $C'(x,0,0)$ is known near the source, equation (21) can be solved directly for the source concentration C_o. For the ideal plume of Figure 6(A), a concentration $C(x,0,0)$ of 977 mg/l is noted at $x = 2{,}400$ cm. Solving

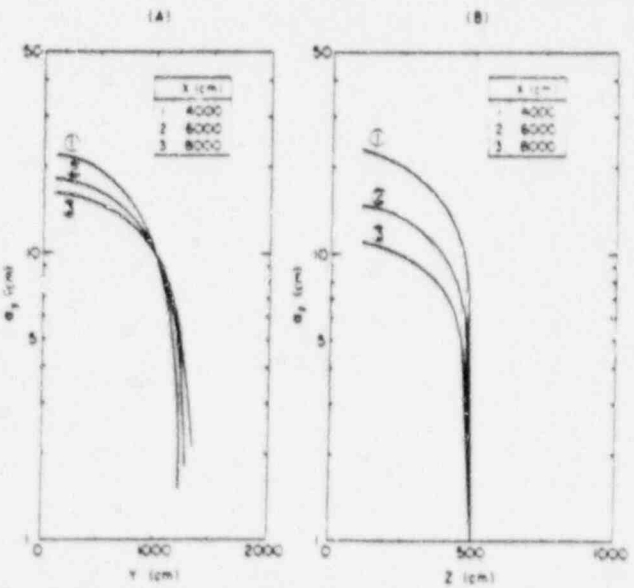

Fig. 7. Plot of (A) the transverse dispersivity α_y versus the source dimension Y and (B) the transverse dispersivity α_z versus the source dimension Z.

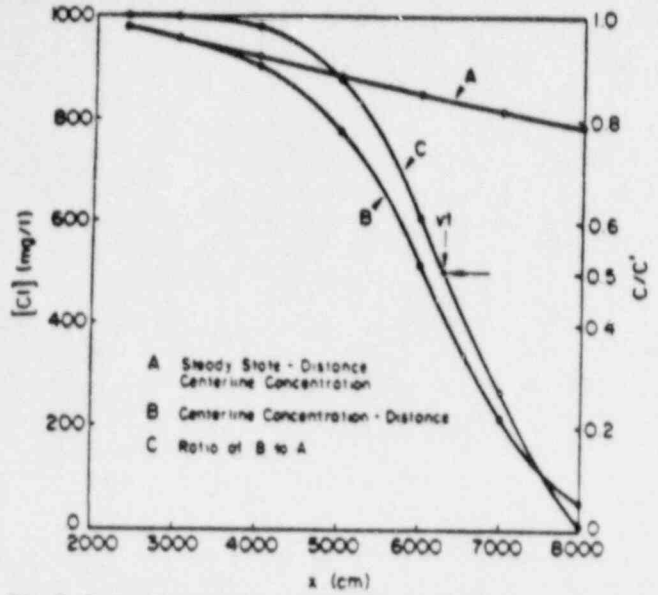

Fig. 8. Centerline concentrations for an ideal plume. Curve A shows steady-state concentrations, curve B shows field concentrations, and curve C is the relative concentration distribution.

equation (21) for C_o gives a source concentration of 999.8 mg/l, which is virtually identical to the designated value. For other concentrations at distances ranging from 1,000 cm to 2,600 cm, equation (21) continually yields a source concentration C_o in excess of 999.6. With all of the variables in equation (21) now known, this equation may be used to determine steady-state concentrations at any x along the centerline. The results of this calculation are shown in Figure 8. In this figure, the curve labeled B represents actual centerline concentrations for the ideal plume of Figure 6, and the curve labeled A depicts steady-state concentrations as determined with equation (21). Curve C is the relative concentration profile developed by taking the ratio of curve B to A, which has the form

$$C(x,0,0,t)/C'(x,0,0) = (\tfrac{1}{2})\,\mathrm{erfc}\,[(x - vt)/2(\alpha_x vt)^{1/2}] \quad \ldots\ldots (22)$$

Equation (22) states that the ratio of actual to steady-state concentration at any x along the centerline of the ideal plume will be equal to one-half the value of the stated complementary error function. Thus, if the actual concentration is already at steady state, which can only occur where $x << vt$, the value of erfc approaches two, and the ratio C/C' approaches unity. From Figure 8 it is clear that the ideal plume is at steady state in the region from x equals zero to x equals approximately 3,000 cm. On the other hand, when x is set equal to vt, equation (22) states that the location of the center of mass (vt) will always be at some unique distance x where the concentration ratio C/C' equals 0.5. From Figure 8, the center of mass is determined to be at x = 6,300 cm, which corresponds to the distance predicted by the known velocity (10^{-4} cm/sec) and the known time (two years, or 6.3×10^7 sec). As the velocity v is understood to be the velocity of the contaminant, this procedure can be used for both attenuated and unattenuated contaminants without the necessity of retardation factors. If the plume is mapped at two different points in time, both velocity and time (as opposed to their product only) may be determined. For the case of an attenuated species mapped at two different points in time, the retardation factor is easily found by taking the ratio of the respective distances x = vt, as determined above.

The last remaining unknown, α_x, is readily determined with equation (22) and Figure 8 for any x in the unsteady portions of the plume. For points behind the determined vt of 6,300 cm, α_x averages 98.9 cm; for points in front of the determined vt, α_x averages 101.5 cm. The overall average is 99.8 cm, which compares favorably with the stipulated value of 100 cm. Indeed, if the actual value of vt was used (6,307.5 cm), all of the points employed above would yield an exact value of 100 cm. Thus, if the position of the center of mass is underestimated, however slight, an exact match in the unsteady portions of the plume requires a scaling up of α_x in front of vt, and a scaling down in the region behind vt. Presumably, the amount of scaling required will depend on the degree of error in determining the position of the center of mass. It is noted that the methods employed above do not require knowledge of the seepage velocity nor the time in ascertaining this position.

The procedures described above represent a systematic approach to obtaining the pertinent transport parameters and coefficients more or less independently of each other. These include the transverse dispersivities α_y and α_z, the source dimensions Y and Z, the source concentration C_o, the distance traveled by the center of mass vt, and the longitudinal dispersivity α_x. Unfortunately, the data demands are rather large and require concentrations within a given plane of a well-defined three-dimensional plume. If the field concentrations are not within this single plane but are determined at various depths for a three-dimensional problem, the point of uniqueness demonstrated on Figure 7 will not materialize. Indeed, when dealing with real data, an exact

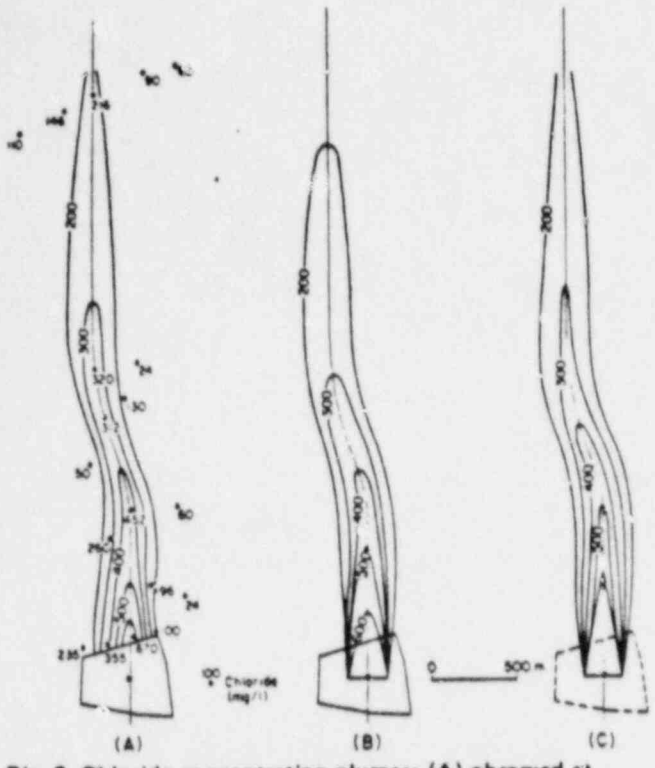

Fig. 9. Chloride concentration plumes: (A) observed at refuse tip, (B) reproduced by extended pulse model with α_y = 4 m and Y = 200 m, and (C) reproduced by extended pulse model with α_y = 2.65 m and Y = 220 m.

adherence to the idealized behavior shown on Figure 7 is not likely. Nevertheless, it is a worthwhile exercise to treat the data in this fashion to obtain reasonable bounds on the transverse dispersivity, and especially so if the source size is known already from other data.

A FIELD EXAMPLE

As a demonstration of a field application of the methodology discussed, a ground-water contamination study by Exler (1972) is used. The waste facility is believed to have been first put into operation in 1954. For this analysis, 1970 data are employed, where observation points extend to almost 3,500 m from the source, where surprisingly large concentrations are encountered. The spreading geometry is considered to be of the type already discussed in the construction of Figure 6.

The available data base and some contoured representation is shown in Figure 9(A). A groundwater mound exists beneath the refuse site, the center of which is taken as the point of origin for the plume. As noted, very little data are available in general and especially so in the upper one-third of the plume. The plume narrows considerably in its central portions and is not perfectly symmetrical near the source. The reasons for the narrowing are likely related to the geology of the transporting medium, which is reported to be marly clay with interlayers of sand. The plume obviously follows the favored pathways in sand and, where the pathways are not laterally extensive, the transverse spreading is constrained.

The relationship between the source dimension Y and the transverse coefficient α_y is shown in Figure 10. In the absence of actual data, contour values had to be used in this iteration, with most of the analysis taking place within three source sizes where control was the most abundant. As anticipated, uniqueness between Y and α_y was not obtained. On the positive side, however, the intercepts on the α_y axis become higher (greater) with decreasing distance from the source, as expected under ideal behavior (Figure 7). Further, upon closer observation, it is noted that α_y can vary from 1.85 m to 7.5 m over a source dimension variation of 225 m to 170 m. In general, the lowest α_y values and the largest source size determinations are from the data points furthest from the source. The relationships shown on Figure 10 are perhaps the best that can be expected under these conditions where the data are very sparse to the extent that contoured values had to be employed, and the geology very complex. Averaging the results of Figure 10 suggests an average α_y on the order of 4 m for a source dimension Y on the order of 200 m.

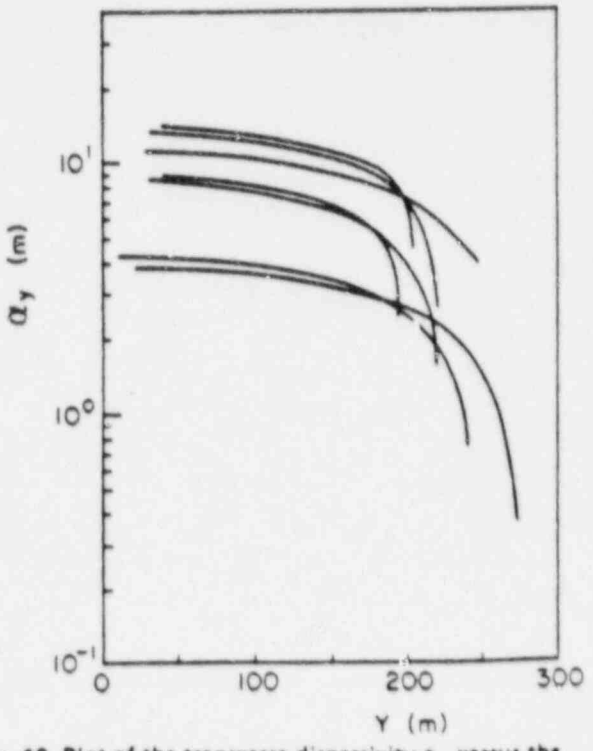

Fig. 10. Plot of the transverse dispersivity α_y versus the source dimension Y at various distances x for the chloride concentration plume.

In the absence of three-dimensional data, the transverse coefficient α_z and the source dimension Z was obtained by the procedures outlined in equations (19) and (20), averaging about 0.0064 m and 5 m, respectively. Vertical dispersion is obviously somewhat insignificant.

In accordance with the procedures outlined earlier, a plot such as Figure 8 is in order, where both the position of the center of mass vt and the longitudinal dispersivity α_x are determined. However, the results of such a plot indicate that the entire plume as mapped on Figure 9 is already at steady state throughout its length; that is, the concentrations are at their maximum values. This agrees with data presented by Exler (1972) who calculated the average velocity to range between 5 to 10 m day^{-1}. Even at one m day^{-1} for a 16-year plume, the center of mass would be located about 5,760 m from the source, or some 2,300 m beyond the last data points of Figure 9. This virtually assures steady state in the mapped region.

The steady-state ideal plume is presented in Figure 9(B) for α_y = 4 m; Y = 200 m, and α_z and Z as previously reported. As noted, the near field matches quite well, which is not surprising in that most of the data used in the analysis came from near-field observation points. In the far field, the 200 mg/l contour is not sufficiently extensive to match the real response. Reducing α_y to 2.65 m for a source size of 220 m, which corresponds to data points of Figure 10 which are furthest from the source, provides the plume of Figure 9(C). Here, the near-field model results start to depart from actual concentrations whereas the far field appears to be accurately depicted. From a simulation perspective, the results appear to be acceptable for a transverse dispersivity on the order of 3 m and a source dimension Y of about 220 m.

CONCLUSIONS

The methodology presented in this paper may be useful in the analysis of contaminant plumes. The calculations are relatively straightforward and easily programmed for microcomputer analysis, and the model can be manipulated to account for several spreading geometries. Most importantly, information on seven potential unknowns can be extracted directly from the concentration distribution, thereby providing a better physical basis for the model. It is argued that such procedures remove much of the nonuniqueness associated with contaminant plume analysis. As the information for the analysis is taken directly off the plume, the method can be applied to chemically retarded species without any regard to retardation coefficients.

On the negative side, the model has limitations common to all analytic expressions, namely the isotropic and homogeneous assumptions along with an assumed constant velocity system. In addition, the data demands are rather large, and the calibration procedure discussed should be viewed as a first try estimate based on an extended pulse approximation that realistically cannot be expected to adequately describe all portions of a plume.

REFERENCES

Baetsle, L. H. 1969. Migration of radionuclides in porous media. In Progress in Nuclear Energy, edited by A.M.F. Duhamel, Series XII, Health Physics. Pergamon, Elmsford, New York. pp. 707-730.

Bruch, J. and R. Street. 1967. Two dimensional dispersion. J. Sanitary Eng. Div., Proc. Am. Soc. Civ. Eng. v. 93, pp. 17-38.

Carslaw, H. S. and J. C. Jaeger. 1959. Conduction of Heat in Solids. Oxford University Press, New York. p. 56.

Cleary, R. W. 1978. Report on 208 Long Island pollution study. Water Resources Program, Princeton University.

Crank, J. 1979. The Mathematics of Diffusion. Clarendon Press, Oxford University Press, New York. pp. 13-15.

Domenico, P. A. and V. V. Palciauskas. 1982. Alternative boundaries in solid waste management. Ground Water. v. 20, pp. 303-311.

Exler, H. J. 1972. Defining the spread of groundwater contamination below a waste tip. In Groundwater Pollution in Europe, edited by J. A. Cole. Water Information Center, Inc., Port Washington, N.Y. pp. 215-241.

Hunt, B. 1978. Dispersive sources in uniform groundwater flow. J. Hydraul. Div., Proc. Am. Soc. Civ. Eng. v. 104, pp. 75-85.

Ogata, A. 1970. Theory of dispersion in a granular medium. U.S. Geol. Survey Prof. Paper 411-I. pp. 12-34.

Prakash, A. 1982. Groundwater contamination due to vanishing and finite size continuous sources. J. Hydraulic Div., Proc. Am. Soc. Civ. Eng. v. 108, pp. 572-590.

Wilson, J. L. and P. J. Miller. 1978. Two dimensional plume in uniform groundwater flow. J. Hydraul. Div., Proc. Am. Soc. Eng. v. 104, pp. 503-514.

* * * * *

P. A. Domenico is currently Harris Professor of Geology at Texas A&M University. He was formerly Professor of Geology at the University of Illinois at Urbana during the period 1968 to 1982, and previous to that time was a Research Associate Professor at the Desert Research Institute, University of Nevada at Reno.

G. A. Robbins has recently joined Woodward-Clyde Consultants in Santa Ana, California as a Senior Project Geohydrologist. He has been employed by the U.S. Nuclear Regulatory Commission and, until very recently, by Texas A&M University as Associate Professor of Geology.

```
      program disp
cc
c iteratively find the location of a specified concentration
c along a plume from user-specified alpha's, thickness,
c width, and possible time
cc
      character *20 fname
      parameter(tol=1.e-5)

      write(*,*) ' enter the file name '
      read(*,'(a)') fname
      open(10,file=fname)
      write(10,1000)

 5    write(*,*) ' enter the concentration ratio'
      read(*,*) cr0
      if(cr0.eq.0) then
        close(10)
        stop
      endif
      write(*,*) ' enter the time '
      read(*,*) t
      if(t.lt.0.) then
        write(*,*) ' enter Alphay'
        read(*,*) alphay
        write(*,*) ' enter Alphaz'
        read(*,*) alphaz
      else
        write(*,*) ' enter the velocity'
        read(*,*) v
        write(*,*) ' enter Dx '
        read(*,*) dx
        write(*,*) ' enter Dy '
        read(*,*) dy
        write(*,*) ' enter Dz '
        read(*,*) dz
        fx=1/(2.*sqrt(dx*t))
        alphay=dy/v
        alphaz=dz/v
      endif

      write(*,*) ' enter the width'
      read(*,*) y
      write(*,*) ' enter the thickness'
      read(*,*) z


      x1=1000.
      x2=1010.
 7    write(*,*) ' enter x1,x2'
      read(*,*) x1,x2
      yo4=y/4.
      zo4=z/4.
      crt1=erf(yo4/sqrt(alphay*x1))*erf(zo4/sqrt(alphaz*x1))
      crt2=erf(yo4/sqrt(alphay*x2))*erf(zo4/sqrt(alphaz*x2))
      if(t.gt.0.) then
        crt1=.5*erfc((x1-v*t)*fx)*crt1
        crt2=.5*erfc((x2-v*t)*fx)*crt2
      endif
 10   cre1=crt1-cr0
      cre2=crt2-cr0
      write(*,*) ' x1 = ',x1
      write(*,*) ' x2 = ',x2
```

Original is LATB

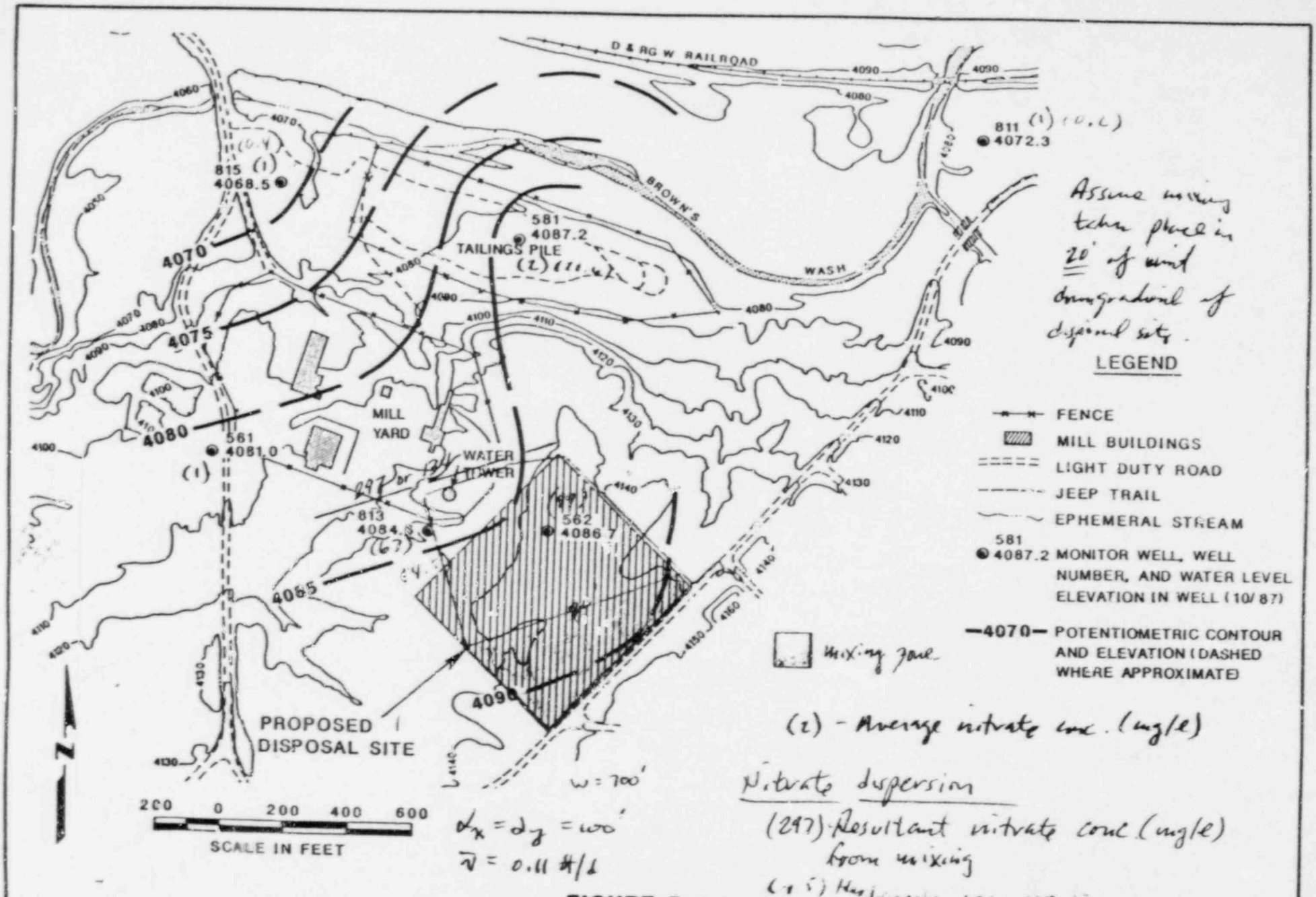

FIGURE D.5.9

POTENTIOMETRIC CONTOUR MAP AND MONITOR WELLS, LOWER - MIDDLE HYDROSTRATIGRAPHIC UNIT, GREEN RIVER , UTAH, TAILINGS SITE, OCTOBER, 1987

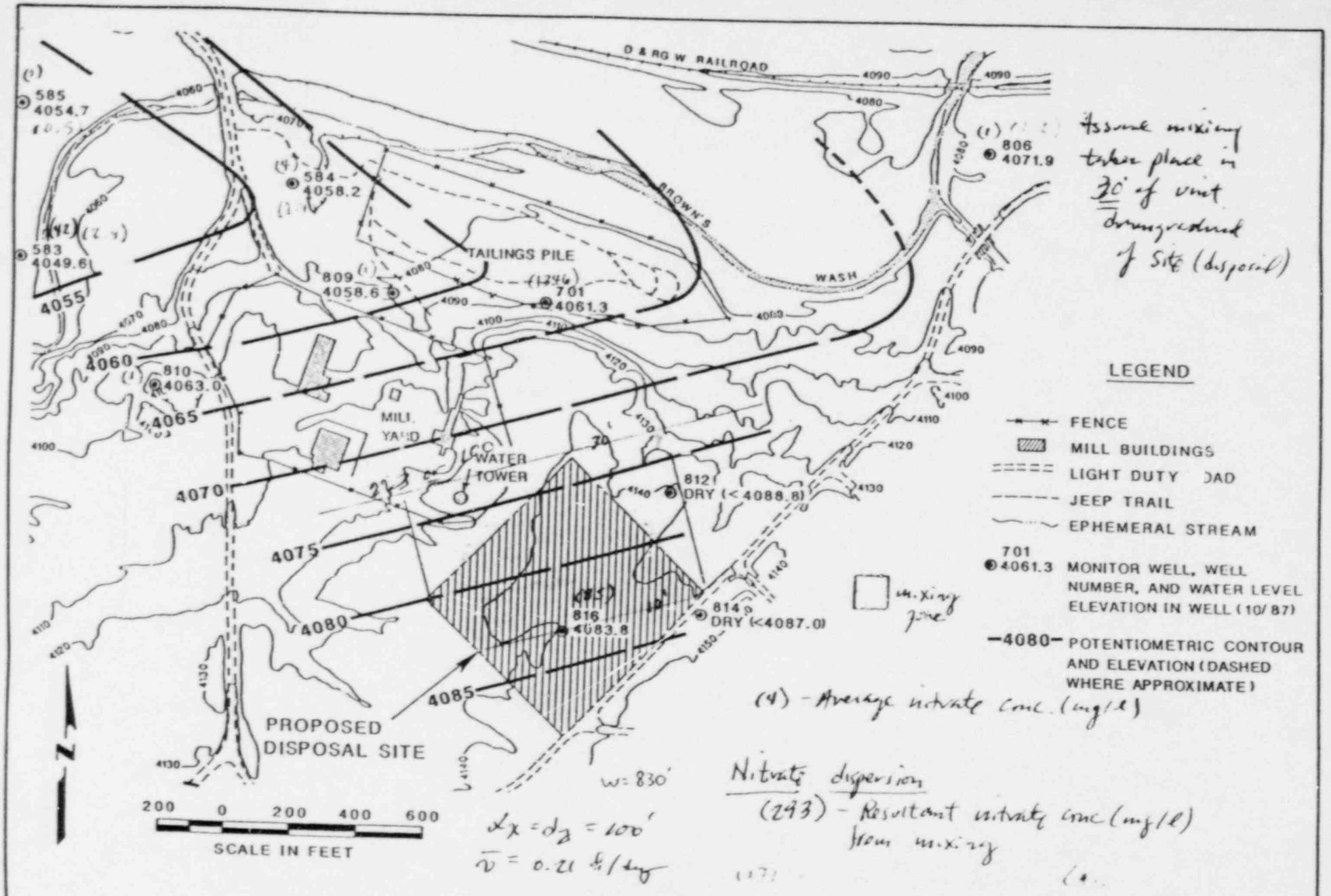

FIGURE D.5.8

POTENTIOMETRIC CONTOUR MAP AND MONITOR WELLS, UPPER – MIDDLE HYDROSTRATIGRAPHIC UNIT, GREEN RIVER, UTAH, TAILINGS SITE, OCTOBER, 1987

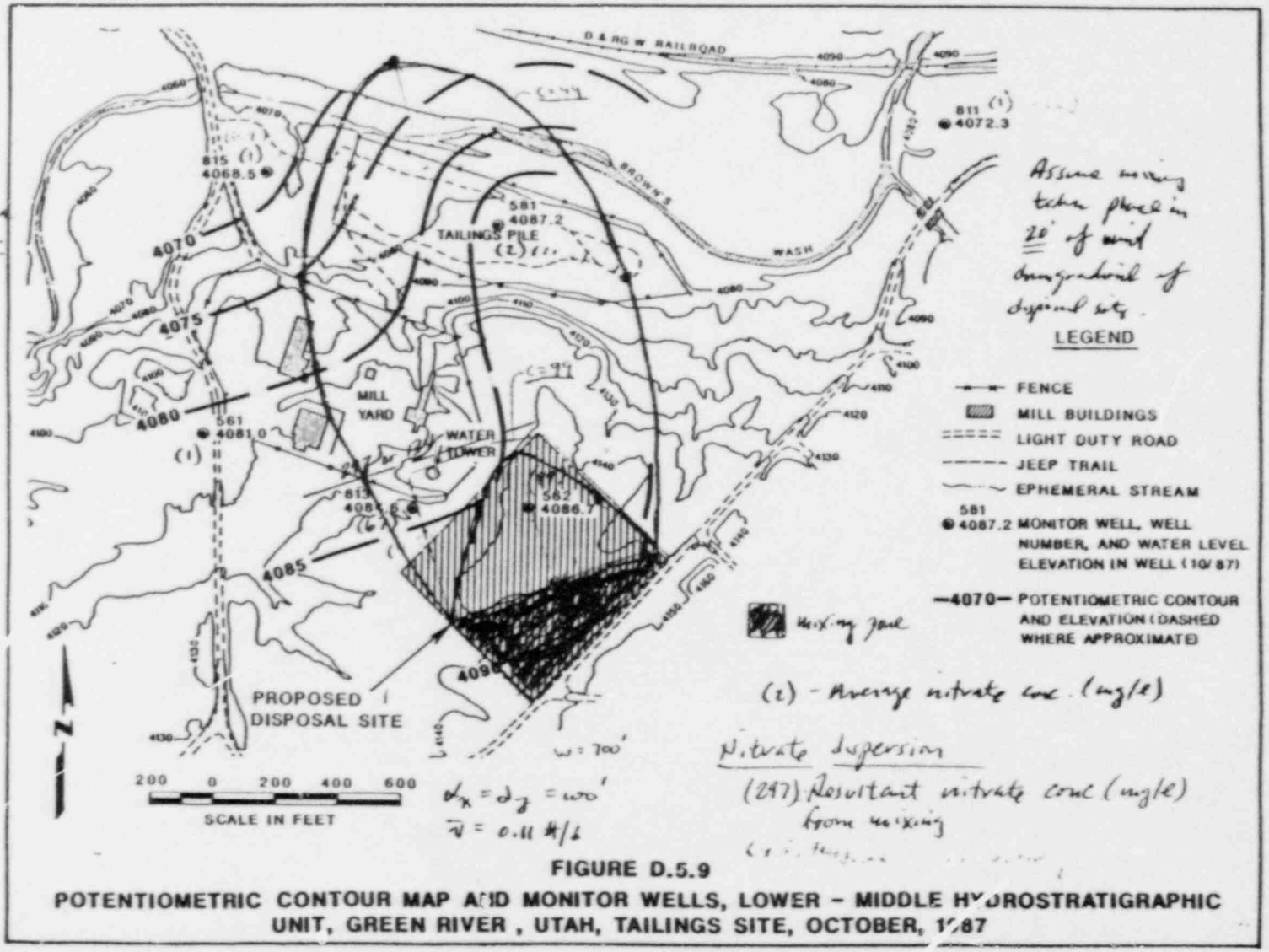

FIGURE D.5.9

POTENTIOMETRIC CONTOUR MAP AND MONITOR WELLS, LOWER – MIDDLE HYDROSTRATIGRAPHIC UNIT, GREEN RIVER , UTAH, TAILINGS SITE, OCTOBER, 1987

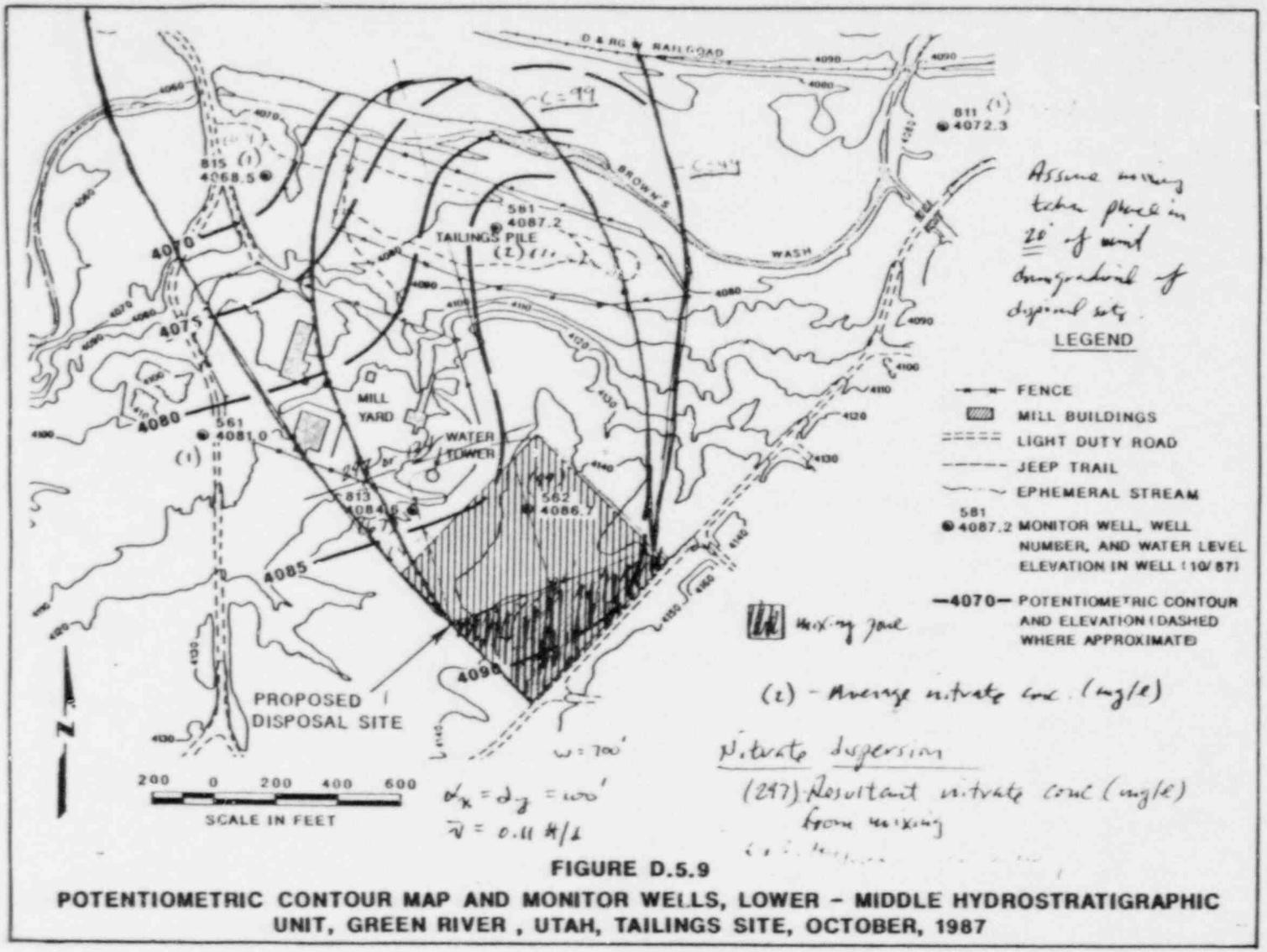

FIGURE D.5.9

POTENTIOMETRIC CONTOUR MAP AND MONITOR WELLS, LOWER - MIDDLE HYDROSTRATIGRAPHIC UNIT, GREEN RIVER , UTAH, TAILINGS SITE, OCTOBER, 1987

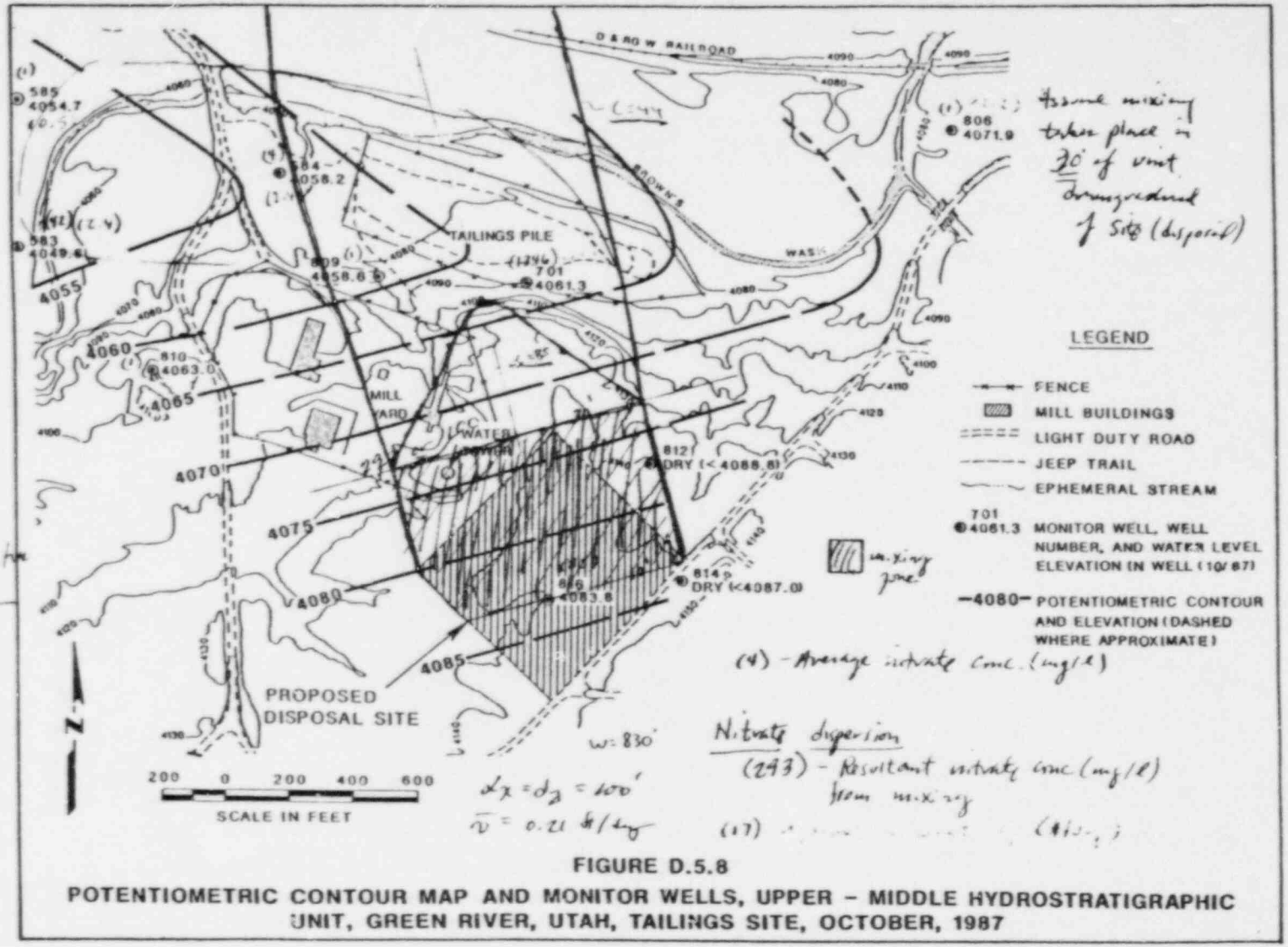

FIGURE D.5.8

POTENTIOMETRIC CONTOUR MAP AND MONITOR WELLS, UPPER – MIDDLE HYDROSTRATIGRAPHIC UNIT, GREEN RIVER, UTAH, TAILINGS SITE, OCTOBER, 1987

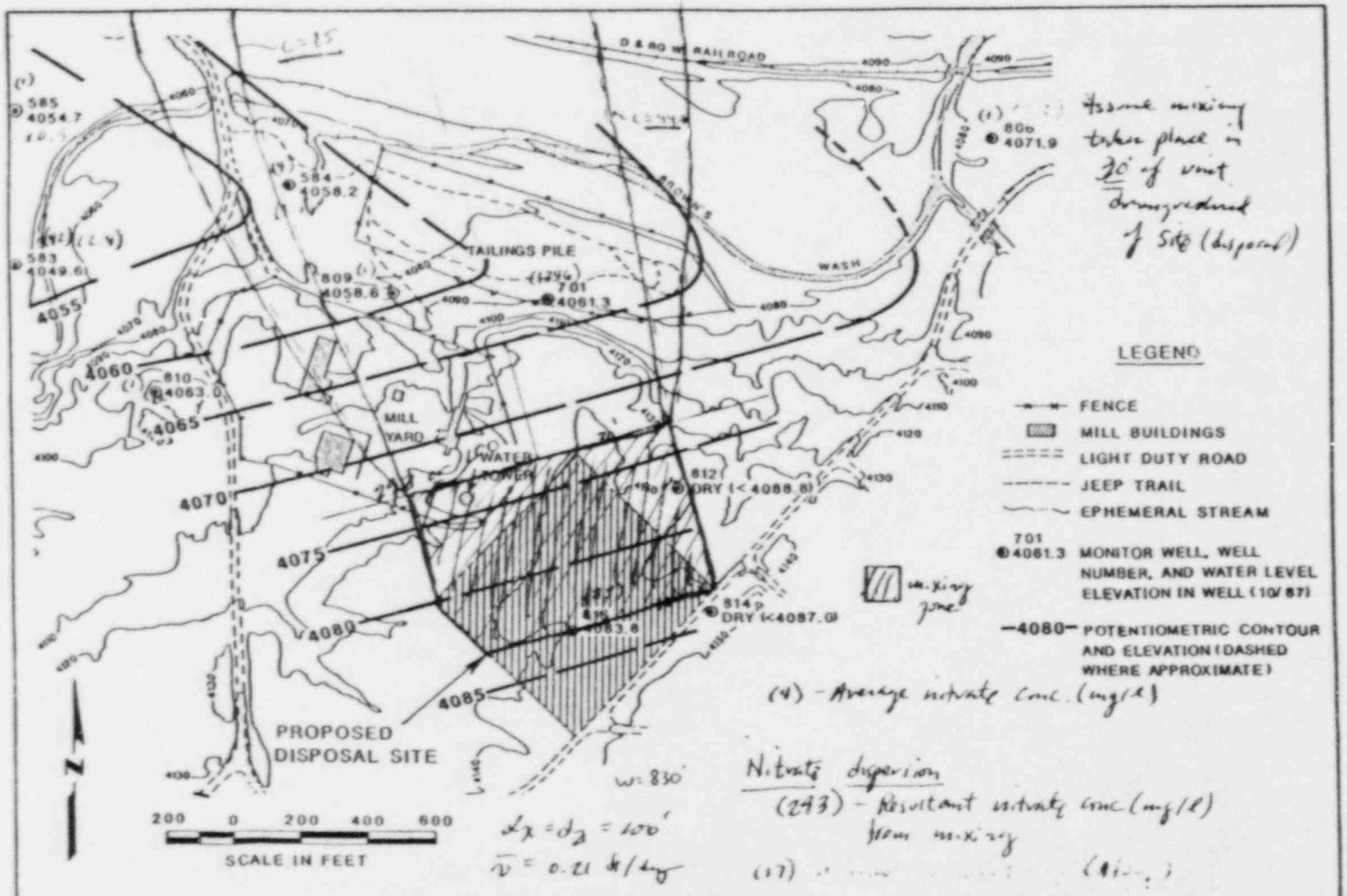

FIGURE D.5.8

POTENTIOMETRIC CONTOUR MAP AND MONITOR WELLS, UPPER – MIDDLE HYDROSTRATIGRAPHIC UNIT, GREEN RIVER, UTAH, TAILINGS SITE, OCTOBER, 1987

JACOBS ENGINEERING

DATE Feb 9, 1988 SUBJECT Summary of Domenico - Robbins SHEET NO _____

BY Walt CHKD. _____ Dispersion calculations JOB NO _____

Nitrate - MCL = 44 mg/l

	Lower - middle unit	Upper - middle unit
Velocity	40 ft/yr	74 ft/yr
Regional Bkgnd conc.	1 mg/l	4 mg/l
Local Bkgnd conc.	99 mg/l	85 mg/l
Source conc.	134 - 297 mg/l	100 - 293 mg/l
α_T, α_L	100 ft	100 ft
Width	700 ft	830 ft
Thickness	20 ft	30 ft

Target conc. \ Source conc.	10^{-8} 134	10^{-7} 297
44	.32	.15
99	.74	.33

Target conc. \ Source conc.	10^{-8} 100	10^{-7} 293
44	.42	.18 .14
85	.84	.37 .28

C/C$_0$ = $\frac{\text{Target - Reg'l Bkgnd}}{\text{Source - Reg'l Bkgnd}}$

Target Conc. \ Source conc.	10^{-8} 134	10^{-7} 297
44	1740'	4250'
99	435'	1670'

Target conc. \ Source conc.	10^{-8} 100	10^{-7} 293
44	2430'	10600' 7700
85	440'	4490' 2700

D* - distance to disperse to target concentration, ft

Target conc. \ Source conc.	10^{-8} 134	10^{-7} 297
44	510'	890'
99	210'	500'

Target conc. \ Source conc.	10^{-8} 100	10^{-7} 293
44	460'	1130' 950
85	205'	680' 530

W* - plume half-width at 1/2 D*

JACOBS ENGINEERING

DATE 02-09-88 SUBJECT Domenico - Robbins Dispersion GRW SHEET NO

BY LMC CHKD JOB NO

Input V-m unit

$\alpha_x = 100$ ft

$\alpha_x = \alpha_y = 100$ ft

velocity $v = \frac{\bar{k} i}{\eta}$

$\bar{k} = 1.6$ ft/day

i 15'/100' = 0.02 %

$\eta = 0.15$

$v = \frac{1.6 \text{ ft/day } (0.02)}{.15} = 0.21$ ft/day

L-m unit

Input

$\alpha_x = \alpha_y = 100'$

velocity $v = \frac{\bar{k} i}{\eta}$

$\bar{k} = 1.7$ ft/day

$i = 10'/100' = 0.013$ %

$\eta = 0.20$

$v = \frac{1.7 (0.013)}{0.20} = 0.11$ ft/day

JACOBS ENGINEERING

DATE 02-09-88 SUBJECT Average nitrate Conc's SHEET NO 1

BY LZM C CHKD. 6RN JOB NO

U-4 Unit

Well No.		Average
583	14 + 71 + 40 =	42
584	5 + 0.4 + 5.8 =	4
585	1 + 0.4 + 1 =	1
809	1 =	1
810	1 =	1
701	1370 + 1190 + 570 + 2480 + 1120 =	1346
806	1 =	1
807	670 =	670
816	85 =	85

L-4 Unit

Well No.		
561	.3 + 1 + .1 + 1 =	1
562	45 + 66 + 130 + 133 + 173 =	99
811	1 =	1
813	47 =	47
581	4.2 + 0.4 + 1.0 =	2
815	1 =	1

Note: compilation of unknown & reference

TABLE A-6

Dispersivity of the Alluvial Aquifer at Several Sites at Lyons, France

Method	Mean velocity (V) ft/day	m/day	Longitudinal dispersivity (α_x) (ft)	(m)	Longitudinal dispersion ft^2 $(D_x)_m^2$ /day	/day	Dispersion Ratio α_x/α_y or D_x/D_y
Single-well test			.33-1.6 (stratum scale)	0.10-0.50			
			16 (full aquifer)	5.0			
Single-well test with resistivity	24	7.2	40	12.0	960	292.6	0.9-3.9
	32	9.6	26	8.0	832	253.6	8.0-530
	43	13.0	16	5.0	688	209.7	0.34-34.5
	30	9.0	23	7.0	690	210.3	7.0-780
Environmental t			40	12.0			3.0

TABLE A-7

Dispersivities From Two-Well Tests

Type of Aquifer	Location	Distance between wells (m)	Porosity	Dispersivity (m)
Fractured dolomite	Carlsbad, N.M.	38.1-54.9	0.12	38.1
Fractured schist & gneiss	Savannah Riv. Plant, S.C.	538	0.0008	134.1
Alluvial sediments	Barstow, CA	6.4	0.40	15.2
Alluvial sediments	Tucson, AZ	79.2	0.38	15.2
Fractured Chalk	Dorset, Eng.	8	0.005	3.1
Chalk	Dorset, Eng.	8	0.023	1.0

Regional Dispersivities (a)

Type of aquifer	Location	Porosity	Longitudinal dispersivity (a_x) (ft)	Dispersion ratio (a_x/a_y (or) D_x/D_y)
Alluvial sediments	Rocky Mountain Arsenal, Colo.	0.30	100	1.0
	Colorado	0.20	100	3.3
	California	NR	100	3.3
	Lyon, France	0.2	40	3.0
	Barstow, CA	0.40	200	3.3
	Sutter Basin, CA	0.05-0.2	260-6600	10.0
Glacial deposits	Long Island, N.Y.	0.35	70	5.0
Limestone	Brunswick, GA	0.35	200	3.3
Fractured basalt	Idaho	0.10	300	0.7
		0.10	300	1.0
	Hanford site, Washington	NR	100	1.7
Alluvial sediments	Barstow, CA	0.40	200	330.0
	Alsace, France	NR	49	15.0
Glacial till	Alberta, Canada	0.001 and 0.53	10-20	5.0
Limestone	Cutler area, Fla.	0.25	22	10.0
	Hypothetical	0.10	0.01-100	5.0
		0.3	70	5.0
		0.02-0.2	33	-
		0.3	1.6-330	1.0-20.0

Radioactive and Biological Decay

Decay of radioactive species is part of the natural attenuation mechanism. The prime interest is the half-life of the species involved. Table A-9 was assembled from standard textbooks on the subject. Other isotopes can be found in the literature if needed.

Note – SOILMOIST runs were for "worst-case" (unrealistic case) scenario of year-round saturation of the upper bedding layer (e.g., no evaporation); see final ¶ of discussion. Lee

1 SIMULATION

```
**********  ********************************************
*                                                      *
*  ONE DIMENSIONAL UNSATURATED TRANSIENT FLOW MODEL    *
*                                                      *
********************************************************
```

Green River - 1'st slope break, top half, backfill char. 95%, Maulem, T3

********** INPUT DATA **********

OPTIONS = 110100000
MAXIMUM CHANGE IN MOISTURE CONTENT OVER A TIME STEP IS .00100
STORAGE COEFFICIENT FOR SATURATED LAYERS IS .000000
INITIAL INTEGER RANDOM NUMBER SEED= 47
INITIAL TIME STEP IS (DAYS) 1.0000000
TIME STEP WILL INCREASE BY A FACTOR OF 1.5000000
DURATION OF SIMULATION IS 10 YEARS

TOTAL NUMBER OF LAYERS IN PROFILE IS 15
TOTAL SOIL PROFILE THICKNESS IS 30.0 CENTIMETERS
DISTANCE FROM BASE OF PROFILE TO WATER TABLE IS 50.00 FEET

PROPERTIES OF THE EROSION BARRIER ARE:
THICKNESS (CM.)= 15.200
SATURATED HYDRAULIC CONDUCTIVITY(CM/SEC)= .10000E-01
SLOPE= .50000E-01
POROSITY= .25000
AVERAGE SLOPE LENGTH (FEET) = 95.000
THE AVERAGE TIME OF INFLOW (DAYS) = 14.757

SOIL TYPE	NO. OF LAYERS	LAYER THICKNESS (CM)	PRESSURE POTENTIAL (BARS)	SOIL POROSITY	SATURATED MOISTURE CONTENT(%)
1	15	2.00	-1.200	.364	36.43

SOIL TYPE 1
****

PRESSURE POTENTIAL (BARS)	SOIL MOISTURE CONTENT	PRESSURE POTENTIAL (BARS)	HYDRAULIC CONDUCTIVITY (CM/SEC)
-62.911	.005	-62.911	7.532E-016
-24.957	.009	-24.957	2.702E-014
-9.897	.018	-9.897	9.745E-013
-5.258	.027	-5.258	7.918E-012
-3.918	.037	-3.918	3.505E-011
-2.904	.046	-2.904	1.113E-010
-2.272	.055	-2.272	2.861E-010
-1.844	.064	-1.844	6.364E-010
-1.538	.073	-1.538	1.273E-009
-1.309	.082	-1.309	2.351E-009
-1.131	.092	-1.131	4.072E-009
-.990	.101	-.990	6.703E-009
-.876	.110	-.876	1.058E-008

Upper half of core system

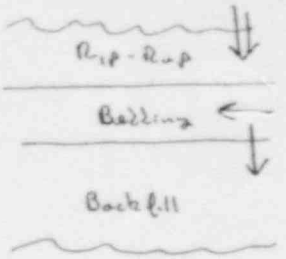

Complete & Original computer print out in LATB